Master's thesis

NTNU
Norwegian University of Science and Technology
Faculty of Medicine and Health Sciences
Department of Clinical and Molecular Medicine

Dagny Sanden Døskeland

Assessing the Role of TDG in the Hippocampus-dependent Memory using Transgenic Mouse Models and rAAV Viral Tools

Master's thesis in Molecular Medicine
Supervisor: Jing Ye
Co-supervisor: Magnar Bjørås
May 2022

NTNU
Norwegian University of Science and Technology

Dagny Sanden Døskeland

Assessing the Role of TDG in the Hippocampus-dependent Memory using Transgenic Mouse Models and rAAV Viral Tools

Master's thesis in Molecular Medicine
Supervisor: Jing Ye
Co-supervisor: Magnar Bjørås
May 2022

Norwegian University of Science and Technology
Faculty of Medicine and Health Sciences
Department of Clinical and Molecular Medicine

NTNU
Norwegian University of
Science and Technology

Abstract

Thymine DNA glycosylase (TDG) is a vital enzyme with dual roles in genome maintenance and epigenetic regulation. Emerging evidence indicates an essential role of TDG in active DNA demethylation. DNA methylation serves an important function in transcriptional regulation by recruiting proteins involved in gene repression or by inhibiting the binding of transcription factors to DNA. DNA methylation has been implicated as a necessary mechanism in long-term memory formation due to its role in transcriptional regulation of genes associated with synaptic plasticity. The role of TDG in demethylation suggests a possible involvement of TDG in long-term memory formation, as this type of memory is dependent on transcriptional regulation. This study investigates the role of TDG-regulated DNA demethylation in hippocampal-dependent memory. More specifically, whether depletion of TDG in the hippocampus leads to alteration in animal behaviour and cognition. I optimised a protocol for TDG depletion in hippocampal neurons using viral tools. Further, I evaluated the behaviour and spatial memory of LoxP-miniTdg mice. This was done by assessing anxiety-related behaviour in the Open Field Test (OFT) and by evaluating spatial memory in the novel preference tests Novel Object Location (NOL) and Y-maze. Lastly, I established a new mouse model with conditional brain-specific TDG depletion. My results suggest that: 1) a viral concentration of 1:20 is optimal for depleting TDG while avoiding difficulties associated with Cre-induced neuronal loss and hippocampal lesions. 2) It is unclear whether the depletion of TDG in hippocampal neurons affects long-term spatial memory, as significant variances were introduced in the groups analysed. 3) Establishment of a new mouse model with conditional brain-specific TDG depletion was successful. This was confirmed by immunohistochemistry (IHC) of Green fluorescent protein (GFP), showing Cre-induced GFP expression, and presumably *Tdg* depletion, in CA1, CA3 and DG. This animal model can be used in future studies to further investigate TDG's role in hippocampus-dependent memory.

Sammendrag

Tymin DNA-glykosylase (TDG) er et enzym med viktige roller i genomisk reperasjon og epigenetisk regulering. Tiltredende bevis indikerer en viktig rolle for TDG i aktiv DNA-demetylering. DNA-methylering har en regulerende funksjon i gentranskripsjon gjennom rekrutering av proteiner involvert i genundertrykkelse, eller gjennom å hemme binding av transkripsjonsfaktorer til DNA. DNA-metylering har blitt implisert som en nødvendig mekanisme for dannelse av langtidshukommelse grunnet sin rolle i transkripsjonregulering av gener som er assosiert med synaptisk plastisitet. TDG's rolle i demetylering implikerer en mulig rolle for TDG i dannelse av langtidshukommelse, siden denne typen hukommelse av avhengig av transkripsjonell regulering. Denne studien undersøker rollen til TDG-regulert DNA-demetylering i hippocampus-avhengig hukommelse. Mer spesifikt, om mangel av TDG i hippocampus fører til endring i adferd og kognisjon hos mus. Jeg optimaliserte en protokoll for fjerning av TDG i hippocampale nevroner ved å bruke virale mekanismer. Videre evaluerte jeg adfersel og hukommelse til LoxP-mini*Tdg*-mus. Dette ble gjort gjennom å måle angst-lignende adferd i OFT og ved å teste romlig hukommelse i preferansetestene NOL og Y-maze. Til slutt etablerte jeg en ny musemodell med betinget fjerning av TDG i hjernen. Resultatene mine tyder på at: 1) en viral konsentrasjon på 1:20 er optimal for å fjerne TDG samtidig som man unngår Cre-indusert nevronisk død og skader i hippocampus. 2) Det er ikke klart om fjerning av TDG i hippocampale nevroner påvirker langsiktig romlig hukommelse, da det ble introdusert betydelige forskjeller innad i gruppene som ble analysert. 3) Etablering av en ny musemodell med betinget hjernespesifikk fjerning av TDG var vellykket. Dette ble bekreftet ved Immunohistokjemi (IHC) av grønt fluoriserende protein (GFP) som viser Cre-indusert GFP-uttrykk, og antagelig fjerning av *Tdg* i CA1, CA3 og DG. Denne dyremodellen kan brukes i fremtidige studier for å videre undersøke TDG's rolle i hippocampus-avhengig hukommelse.

Acknowledgements

I would like to thank my main supervisor, Jing Ye, for thorough and continuous supervision throughout the project. Your constant availability for questions and discussions has been invaluable. Further, I would like to thank my second supervisor Magnar Bjørås for the resources making this project possible. I would also like to thank all members in the research group who made themselves available for questions and discussions. Especially thanks Marion Silvana Fernandez Berrocal for teaching me many of the experimental methods in the lab. I would like to thank Anna Maria Bugaj for her help with statistical analysis, and Nils Hagen for the great help in the Animal facility. I would also like to thank Konstanse Skogøy Innvær for help with staining and imaging. Finally, thanks to family and friends for the support given while completing this master thesis.

Table of Contents

List of Figures

List of Tables

List of Abbreviations

AAV	Adeno Associated Virus
AID	Activation Induced Deaminase
AP	Anterior Posterior
AP-site	Apurinic/apyrimidinic site
APE I	Apurinic/apyrimidinic Endonuclease 1
BDFN	Brain Derived Neurotropic Factor
BER	Base Excision Repair
C	Cytosine
CA	Cornu Ammonis
CamKIIα	Calcium/Calmodulin-dependent protein kinase II alpha
CNS	Central Nervous System

CpGs	CpG Dinucleotides
Cre	Cyclisation Recombination
DG	Dentate Gyrus
DNMT	DNA methyltransferase
DV	Dorsal Ventral
EC	Entorhinal Cortex
eGFP	Enhanced GFP
FACS	Fluorescence-Activated Cell Sorting
FOTS	Forsøksdyrforvaltningens tilsyns- og søknadssystem
G	Guanine
GFAP	Glial Fibrillary Acidic Protein
GFP	Green Fluorescent Protein
HPC	Hippocampus
hSYN	Human Synapsin promoter
IHC	ImmunoHistoChemistry
LoxP	Locus of Crossover P1
MS	Mass Spectrometry
ML	Medial Lateral
NeuN	Neuronal Nuclear Antigen
NOL	Novel Object Location
NOR	Novel Object Recognition
NS	Not Significant
OFT	Open Field Test
PBS	Phosphate-Buffered Saline
PCR	Polymerase Chain Reaction
PFA	Paraformaldehyde
rAAV	Recombinant Adeno Associated Virus
RT	Room Temperature
SAM	S-Adenyl Methionine
SPF	Specific Pathogen-Free
SUB	Subiculum
T	Thymine
TDG	Thymine DNA Glycosylase
TET	Ten-Eleven Translocase
UDG	Uracil DNA Glycosylase
WT	Wild Type
5caC	5-CarboxcylMethylCytosine
5fC	5-FormylCytosine
5hmC	5-HydroxyMethylCytosine
5mC	5-MethylCytosine

1 INTRODUCTION

This introduction will first describe the importance of epigenetic mechanisms in transcriptional regulation. It especially emphasises the role of DNA methylation and demethylation in regulating gene expression. This is done so that the reader better understands the importance of studying the enzymes that regulate the DNA methylation pattern. Further, one of these regulating enzymes, TDG, will be introduced. The dual roles of TDG are shortly described, and TDG's function in active DNA demethylation is explained. Next, dynamic DNA methylation is linked to memory formation, as DNA methylation regulates the transcription of genes with roles in synaptic plasticity [1]. Subsequently, the hippocampus is introduced, as it is an essential brain region in which memory formation is facilitated [2]. Since the goal of this study is to investigate the role of TDG in hippocampal-dependent memory, ways of achieving this are described. First, how functional memory can be assessed with behavioural tasks. Secondly, how conditional gene knockout can be performed to investigate gene function.

1.1 Epigenetic gene regulation - Establishment and removal of DNA methylation patterns

1.1.1 Epigenetics

Essentially all cells in an organism contain the same DNA, but cell type and function differ greatly due to differences in the regulation of gene expression [3]. Cells have the capacity for adaptive gene regulation by epigenetic mechanisms that modulate transcription factor complexes, regulate DNA packing, and dynamically change covalent modifications on histones and DNA [4]. Such epigenetic mechanisms enable hereditable alterations in gene expression patterns without making changes in the DNA sequence itself [3, 5, 6]. The interplay between the epigenetic mechanisms is essential, as the sum of their interactions determines the outcome of gene regulation [7]. DNA methylation is one of the best studied epigenetic mechanisms, and serve important functions in transcriptional regulation. Particularly, DNA methylation helps to provide a variability in gene expression while maintaining the information content of the base [6].

1.1.2 DNA Methylation

DNA methylation refers to the adding of a methyl group to the 5' position of cytosine (C) and occurs primarily on a C positioned in front of guanine (G), forming CpG dinucleotides (CpGs) [3, 8, 9]. Regions rich with CpGs, known as CpG islands, are frequently associated with promoter regions and are characteristically hypomethylated [5, 10, 11]. In contrast, hypermethylation in promoter regions is associated with the repression of gene expression and increased heterochromatin formation [12-16]. The addition of an outward projecting methyl group to C creates a steric interference preventing access for the transcription machinery from binding DNA and initiating transcription [17, 18].

Consequently, the gene will be silenced, and downstream protein expression repressed [7, 19, 20]. Cytosine methylation is catalysed by a class of enzymes known as DNA methyltransferases (DNMTs) that transfers a methyl group from S-adenyl methionine (SAM) to the fifth carbon of a C, forming 5mC [9]. The catalytic members of the DNMT family are usually classified into de novo DNMTs (DNMT3a and DNMT3b) and maintenance DNMTs (DNMT1) [7, 21, 22]. De novo DNMTs are responsible for establishing the initial pattern of methylation during embryonic development [21] (figure 1 a). Maintenance DNMT proteins primarily act upon hemimethylated DNA and are required to maintain and conserve the methylation pattern through replication [22, 23] (figure 1 c).

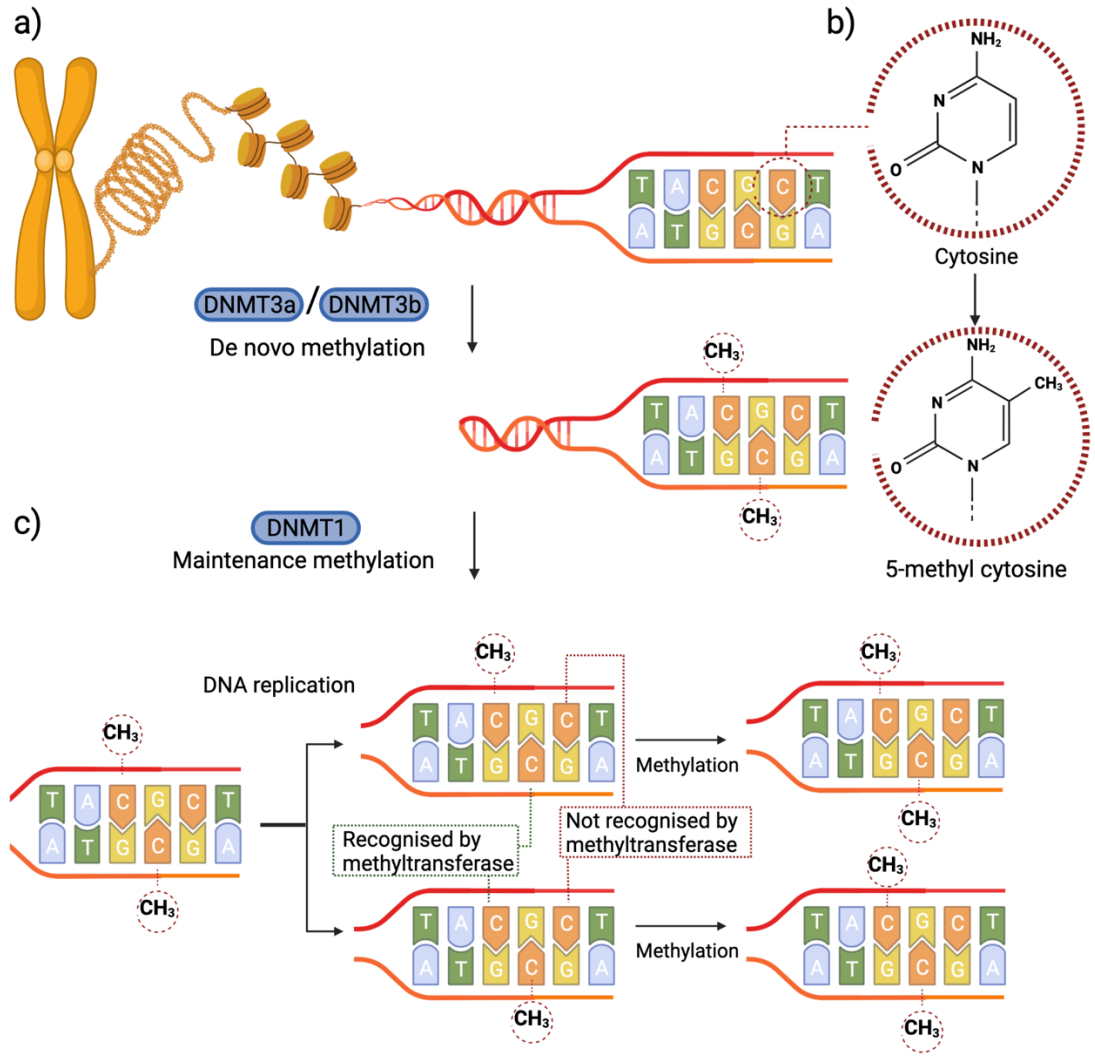

Figure 1. De novo and maintenance methylation of DNA by DNA methyltransferases.

a)The figure shows the initial methylation (de novo) of un-methylated DNA by DNMT3a/DNMT3b. b) The figure shows the conversion of C to 5mC by adding a methyl group. c) The figure shows DNMT1 recreating the parental methylation pattern on hemimethylated daughter strands after DNA replication. The methylation pattern is symmetrically restored as DNMT1 does not recognise and restore unmodified CpGs. Figure created in Biorender.

1.1.3 Demethylation

It has long been thought that DNA methylation profiles in the brain remained static after embryonic development. However, numerous findings indicate a dynamic regulation of the DNA methylation pattern, also after embryonic development [24-26]. 5mC is chemically and genetically stable but can still be reversed into its unmodified state [27]. To enable dynamic alterations in methylation patterns, loss of methyl groups, or DNA demethylation, must occur. Typically, we separate between two processes of DNA demethylation. Namely, the passive or active DNA demethylation processes. Passive DNA demethylation occurs when there is a lack of a functional DNA methylation maintenance machinery, such as DNMT1, which causes a replication-dependent dilution of 5mC [28, 29]. The active DNA demethylation process refers to the active enzymatic removal of methyl groups. While the enzymes that catalyse methylation have been well described in the literature [21, 22, 30], those involved in methyl group removal remain largely uncharacterised, and their molecular mechanism is not fully understood. However, there are several proposed mechanisms in which active DNA demethylation can occur. This includes the pathways of: I) spontaneous deamination of 5mC to thymine (T) followed by base excision repair (BER) of the T· G mismatch (figure 2a), and II) oxidation mediated demethylation by ten-eleven translocase (TET) followed by BER (figure 2b) [31].

I) The spontaneous deamination of 5mC to T by activation-induced deaminase (AID) results in the mispairing of a G and T [32]. The mispaired T is recognised and excised by a mismatch specific Thymine DNA Glycosylase (TDG), creating a lesion that is repaired by the downstream factors of BER [33, 34]. BER is the predominant pathway for correcting small base lesions caused by oxidation, deamination and alkylation [35]. The first step of the BER pathway includes a DNA glycosylase that recognises and excises a damaged or mispaired base, creating an abasic site. The resulting abasic site is repaired by the apurinic/apyrimidinic endonuclease I (APE I) that generates a 3´ OH at the damage site. This is followed by repair synthesis with a DNA polymerase and nick sealing by a DNA ligase [35, 36]. This pathway ensures the correct replacement of the missing nucleotide and ultimately replaces the original 5mC with an unmodified C.

II) Oxidation-mediated demethylation is a process facilitated by TET, an enzyme that iteratively oxidises 5mC to generate 5-hydroxymethylcytocine (5hmC), 5-formylcytosine (5fC) and 5-carboxylcytosin (5caC) [37]. 5hmC is a key intermediate in demethylation, which can be passively depleted through DNA replication or actively converted to cytosine through iterative oxidation and TDG mediated BER [4]. Both the oxidised substrates 5fC and 5caC can be recognised and actively removed by TDG initiated BER [38]. Studies show that accumulation of the TDG recognised substrates 5fC and 5caC is present after TDG depletion in embryonic stem cells and T-cells [39, 40]. TDG's function in demethylation implicates an important role of TDG in the dynamic regulation of methylation patterns, and consequently transcriptional regulation.

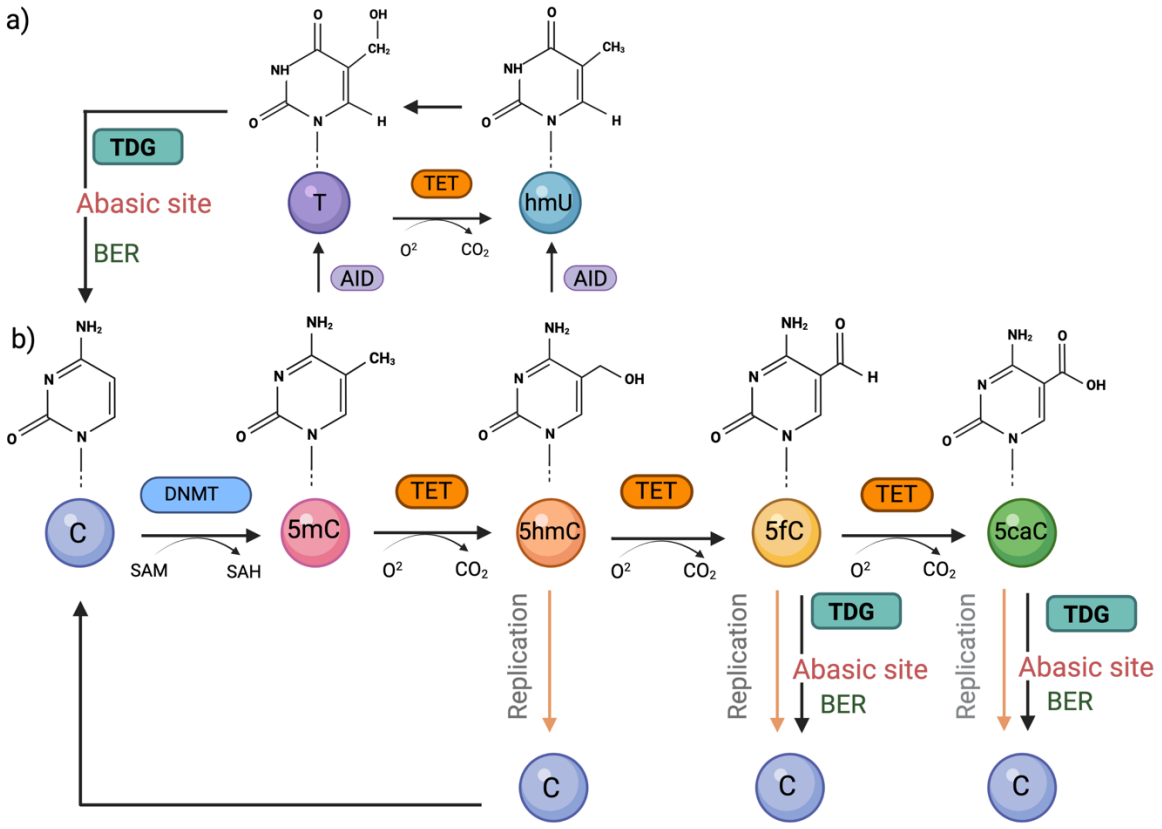

Figure 2. Active DNA demethylation pathways by TDG initiated BER.

DNA methyltransferases (DNMTs) convert unmodified cytosine to 5mC. a)Tthe figure shows the deamination based demethylation pathway where mC is deaminated to T by AID, followed by recognition and removal through TDG initiated BER. b) The figure shows the oxidation based modification and demethylation where mC is iteratively oxidised to 5hmC, 5fC and 5caC by TET dioxygenases. The oxidised substrates 5fC and 5caC are recognised and removed by TDG initiated BER. Orange arrows labelled "Replication" indicate a replication-dependent dilution of 5hmC, 5fC and 5caC. Figure created in Biorender.

1.2 TDG

1.2.1 TDG gene and protein

The human thymine DNA glycosylase (*TDG*) gene is located on chromosome 12q23.3 and has a coding sequence of 3,551 bp that encodes a full-length protein from 10 exons (NCBI Gene ID:6996). Orthologous to the human *TDG*, the equivalent gene in mice (*Tdg*) is located at 10 C1; 10 39.72 cM (NCBI gene ID: 21665). The TDG protein is comprised of 410 amino acids and has a conserved α/β structural conformation [41]. TDG's catalytic domain, referred to as the glycosylase domain, is flanked by N-terminal and C-terminal extensions of variable lengths [42-44]. The catalytic domain modulates the enzymatic activity of TDG, as well as mediating interactions with other proteins, such as nuclear receptors and transcriptional regulators [36, 44-46]. TDG has a general nuclear expression and low tissue specificity. Little is known of its expression pattern in the brain. However, as reported in The Human Protein Atlas, TDG expression has low regional specificity and strong expression in neurons but not glial cells [47](Human Protein Atlas proteinatlas.org).

1.2.2 TDG function

TDG is a member of the uracil DNA glycosylase (UDG) superfamily of DNA repair enzymes and is most known for its essential function in the repair of T·G mismatches [33, 34, 43]. TDG initiates BER by recognising and removing erroneous T·G, and U·G mispairs arising through spontaneous deamination of cytosine and 5-methyl cytosine [48][49]. TDG excises the mispaired base by hydrolysing the N-glycosidic bond of thymine and uracil when mispaired with guanine. This creates a non-destructive DNA lesion (abasic site) that inhibits further DNA polymerase activity and a potential error-prone synthesis [50]. Although TDG is best known for removing T from a T·G mismatch, protein-interaction studies show that TDG interacts with chromatin remodelling factors, transcription factors and DNA methyltransferases [36, 45, 46]. Unlike other DNA glycosylases, TDG is essential for embryonic development, due to its role in transcriptional regulation of developmental genes [51]. Findings report that *Tdg* null embryos are embryonically lethal by E11.5 [51, 52] and that mouse embryonic fibroblasts derived from *Tdg* null embryos have impaired gene regulation, imbalanced histone modification and CpG methylation at promoters of affected genes [51]. Altogether, the evidence demonstrating TDGs role in active DNA demethylation further implicates an essential role of TDG linking DNA repair, control of epigenetic DNA modification, and regulation of gene expression [36, 45, 46].

1.2.3 DNA methylation in learning and memory

DNA methylation serves an important function in transcriptional regulation by recruiting proteins involved in gene repression or by inhibiting the binding of transcription factors to DNA [9]. Dynamic DNA methylation has been implicated as a necessary mechanism in long-term memory formation due to its role in the transcriptional regulation of genes associated with synaptic plasticity. This is supported by numerous studies that show altered transcription of memory activator and suppressor genes after learning experiences. For example, Lonergan et al. show increased expression of the memory enchaining proteins Arc and Zif268 following fear condition [53]. Also, Bekinschtein et al. demonstrate that novel protein synthesis of the memory-enhancing protein Brain-Derived Neurotrophic Factor (BDFN) occurs 12 hours after associative learning tasks [54].

Changes in the DNA methylation landscape after neuronal activity or learning have been observed in genome-wide analysis, revealing that DNA methylation is responsive to increased neuronal activity [55]. For example, Guo et al. show activity-dependent changes in DNA methylation in the adult Dente Gyrus (DG) [56]. This finding was further supported by another study that reported DNA methylation changes in the hippocampal CA1 region after contextual fear conditioning [57]. These findings provide support for the role of DNA methylation in altering the expression of genes involved in synaptic plasticity. Evidence for the role of DNA methylation in memory formation comes from an increasing number of studies that have assessed the effects of the manipulation of DNA methylation modifiers on the formation of memory. The first evidence supporting the idea that dynamic changes in DNA methylation is necessary for long-term memory formation came when Swett et al. reported that treatment with non-specific DNMT inhibitors impaired the formation of contextual fear associations [58]. following this, a study found that inhibition of DNMT activity caused changes in methylation of promoters controlling genes implicated in synaptic plasticity [59]. All together, this supports the

idea that DNA methylation regulates the expression of genes with relevant functions in synaptic plasticity in brain regions critical for memory. Also, dysregulation of the same process occurs in age-associative cognitive decline and pathological conditions such as neurodegenerative diseases, psychiatric disorders and drug addiction [60-62]. This further emphasises the importance of understanding how dynamic DNA methylation regulates long-term adaptations.

1.3 Hippocampus and memory

1.3.1 Hippocampal structure and function

The hippocampus (HPC) is a well-studied brain region due to its critical role in long-term memory formation [63]. The hippocampal formation consists of HPC and the parahippocampal regions, and contributes to the encoding, consolidation and conscious recollection of declarative memory. The hippocampal formation processes a large convergence of sensory signals, as contributed by all sensory modalities [64]. The hippocampus is known to be necessary for the establishment of long-term episodic memory, and play an important role in mapping, modelling and navigation-related spatial memory [65, 66]. Spatial memory is explicit memory specific to spatial locations. The recording of spatial information and its subsequent encoding in the entorhinal-hippocampal spatial representation system constitutes the cognitive process of spatial memory [67, 68].

The hippocampal formation is located deep within the brain's medial temporal lobe and is a part of the limbic structure [69, 70]. The hippocampal formation is generally categorised into substructures based on differences in neuron population and intrinsic and extrinsic connectivity patterns. This includes structures such as the Dentate Gyrus (DG), Cornu Ammonis (CA), the Entorhinal Cortex (EC) and the subiculum (SUB). The hippocampal subregion CA is again divided into subregions CA1- CA3 [71, 72]. The hippocampal trisynaptic circuit enables the acquisition of spatial and episodic memories by linking the HPC with neocortical areas involved in sensory perception, cognition and spatial reasoning [73, 74]. Sensory input primarily travels through the EC, where local fibre bundles connect and project signals to the granule cells of the DG via the perforant pathway [73, 75]. The pathway continues as DG transmits the signal to the CA3 pyramidal cells through mossy fibres (the axons of DG granule cells), forming the second part of the pathway. Finally, the signal continues from CA3 pyramidal cells to the CA1 Schaffer collateral neurons, completing the trisynaptic circuit (Figure 4) [76]. Signals from CA1 also travel from the HPC to other brain regions by projection through the EC and the SUB [77, 78].

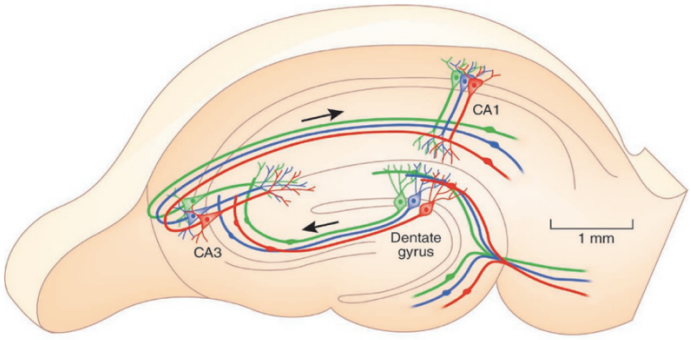

Figure 3. Hippocampus and the Trisynaptic Patway.

Illustration of the main hippocampal circuitry of the DG and CA. Input from the EC travels to the DG via the perforant pathway, and connections from DG to CA3 travel through the Mossy Fibres. Figure created by Katie Vicari and obtained from Edvard Moser et al. "The multi lined hippocampus" [79].

1.4 Assessing functional spatial memory by behavioural tests

Our ability to orient ourselves in an environment depends on our ability to learn and remember locations. Creating a spatial memory is normally based on two systems. The allocentric navigation system that uses cues outside the organism (distal cues) and the egocentric navigation system that uses self-movement, internal cues, and nearby proximal cues [80]. The primary region essential for allocentric navigation is the HPC. Functional hippocampal-based spatial memory is often assessed using animal models in behavioural tasks [81]. There are various behavioural paradigms established to assess spatial memory in mice, including T-maze, Y-maze, Morris water maze, and Novel object recognition test, to mention some. Essentially, all these tasks assess functional spatial memory by measuring an animal´s ability to recognise and remember a location or object. Functional spatial memory can be evaluated with behavioural task. To evaluate the role of a specific gene in behaviour and memory, gene knockout, and subsequent behaviour tests can be performed. Impairments in spatial memory have been observed in several studies with a knockout of genes important for memory formation [82-84]. Hence, mice with depletion of genes potentially important for memory formation can be assessed in behavioural tests to evaluate the role of the gene in learning and memory.

1.5 Conditional gene knockout for studying gene functionality

Investigating gene function is often done by observing phenotypical changes after gene knockout. However, conventional gene knockout techniques have some disadvantages. For example, loss of functionally essential genes can result in embryonic lethality, making it impossible to study gene function at later stages of development or in adult animals. Furthermore, a conventional knockout is not time-or tissue-specific, as it causes a simultaneous knockout in the whole animal. Therefore, it can give an inaccurate picture of gene function, as genes have several properties and expression levels depending on

cell type and tissue. To circumvent these difficulties, strategies for conditional gene knockout have been developed.

1.6 Cre-LoxP system

The Cre-LoxP system is a site-specific recombinase technology widely used for genetic editing to facilitate insertions, deletions, and inversions at specific sites in the genome of transgenic mice [85]. Cyclisation recombination, or Cre, is a recombinase derived from the P1 bacteriophage that can recognise and catalyse the recombination between two LoxP recognition sites [86, 87]. LoxP sites consist of a 34 bp consensus sequence with an 8 bp core sequence flanked on each side by a 13 bp palindromic sequence [85]. LoxP sites are introduced into the genome by homologous recombination such that they flank a gene of interest (referred to as a "floxed gene") [88]. When the two loxP sites flanking the gene of interest are oriented in the same direction, the gene will be excised upon Cre activation [89].

Viral gene delivery methods, such as Adeno Associated Viral (AAV) technologies, have shown to be useful for introducing Cre into organisms [85, 90]. Recombinant Adeno Associated Viruses (rAAVs) are modified from wild type AAVs and use an expression cassette to drive transgenic expression [91]. The synthetically created expression cassette can be modified to harbour a promoter and a transgene of choice. Thus rAAVs can be used as an efficient tool for gene delivery giving cell or tissue-specific expression [91]. Typically, the visualisation of viral infection and expression of the transgene is attained by adding a fluorescent reporter gene, such as green fluorescent protein (GFP) [91].

Another common strategy for tissue or cell-specific conditional gene knockout in mice is to breed animals containing a floxed gene with mice carrying a Cre gene downstream of a tissue-or cell-specific promoter. The calcium/calmodulin-dependent protein kinase II alpha (CamKIIα) is a promoter predominantly controlling expression in the cerebral cortex and HPC, and has been utilised for brain-specific inactivation of genes [88, 92]. Studies show that CamKIIα is barely detectible in mice at postnatal day four but increased 10-fold in the frontal cortex by day sixteen [93]. Both of these properties make the CamKIIα an ideal promoter controlling neuron-specific Cre expression, as it gives possibilities for a tissue-and time-controlled inactivation of a floxed gene of interest.

1.7 Aim

In this project, the overall aim is to investigate the role of TDG-regulated DNA methylation in hippocampal-dependent memory. More specifically, whether depletion of TDG leads to alteration in animal behaviour and cognition. To achieve this, I have three main objectives:

1) Optimise a protocol for rAAV-induced TDG depletion in hippocampal neurons
2) Assess animal behaviour and long-term memory of LoxP-mini*Tdg* mice in various behavioural tasks
3) Establishing a brain-specific TDG depletion mouse model

2 METHODOLOGY

2.1 Ethics statement and Animal work

All animal work performed was carried out following the Animal Welfare Act and guidelines directed by the Norwegian Food Safety Authority (Mattilsynet). For details on approval of experimental procedures, see "forsøksdyrforvaltningens tilsyns- og søknadssystem" (FOTS) application with registration number 24310, at mattilsynet.no. Breeding, housing, and experimentation took place in the Comparative Medicine Core Facility at St.Olavs Hospital. All mice were housed in the specific pathogen-free (SPF) unit in individually ventilated cages with a 12h reversed light-dark cycle (light 18:00-06:00) at 23±2°C and 55-65% relative humidity. Diet (Ssniff V1536) and water were provided *ad libitum*, and animal health was assessed daily.

2.2 Mouse models

The transgenic mouse model used in this study contains a loxP-flanked mini-*Tdg* gene and enhanced GFP (eGFP) sequence following a loxP-STOP-loxP cassette (figure 3). By introducing the expression of Cre recombinase, the loxP-flanked mini-*Tdg* and the STOP codon before eGFP are deleted, allowing visualisation of gene depetion. Adult mice (3-6 months old males) are used for virus injection and behavioural studies. Additionally, we established a CamKIIα-*Tdg*-KO mouse line by crossing LoxP-*miniTdg* mice with a Tg(CamKIIα-Cre)T29 mouse strain from Jackson Laboratory.

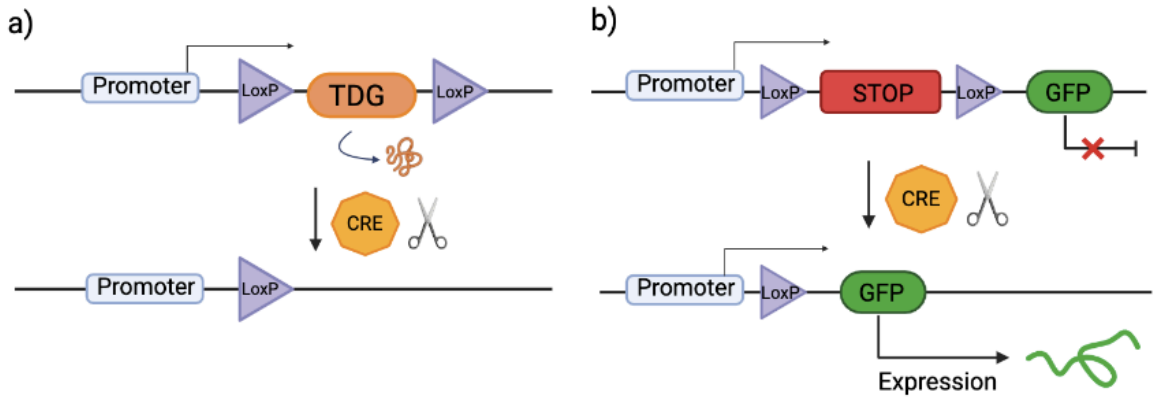

Figure 4. Cre-recombinase dependent excision of miniTDG and GFP stop signal.

a) Figure shows a schematic overview of the loxP flanked miniTdg gene. LoxP sites in the same orientation allow for gene excision by Cre activation. b) The figure shows Cre-dependent expression of the fluorescent reporter gene GFP. A floxed stop signal removed by induction of Cre recombinase enables the expression of the fluorescent GFP protein. Figure created in Biorender.

2.3 Genotyping

Genotyping was verified through Polymerase chain reaction (PCR) using genomic DNA from mouse ear biopsies. Ear samples were lysed with lysis buffer (10mM Tris, 1M KCl, 0,4% NP-40/Igepal CA630 Sigma, 0,1% Tween20) and protein kinase K (10 mg/ml) before being incubated at 60°C overnight. Subsequently, samples were heated at 95 °C for 30 min, followed by centrifugation for 20min at 14000rpm. In a total volume of 10µl, DNA preparations (diluted 1:10 in ddH_2O) were combined with Taq 2X Master Mix (10xPCR buffer, 2.5 mM dNTPs, 5U/µl paq5000, 50 mM $MgCl_2$), ddH_2O and 0,5µm of each primer pair for either *miniTdg*, eGFP, wild type (WT) or Cre, depending on strain analysed (see appendix table 1 for details on primer sequences). PCR settings were set to 3 min at 95°C, 30sec at 95°C, 42X (30sec at 64°C, 30sec at 72°C), followed by a 1 min extension at 72°C before holding at 4°C ∞. PCR products were separated by electrophoresis in a 2% (w/v) agarose gel. The gel was prepared with agarose (BioNordika LE Agarose), TAE buffer (Tris base, Glacial Acetic Acid, 0,5 EDTA), and 0,001% SybrSafe (Thermoficher/Invitrogen). A 100bp DNA ladder was used to determine the size of the PCR product. PCR product, together with 6X DNA loading dye (New England Biolabs), was loaded into the gel before it was run at 120V for 40min. Results were visualised in UV exposure by the ChemiDoc™MP imaging system (BIORAD).

2.4 Surgical procedure and virus injection

rAAV carrying the human synapsin promoter (hSYN) was be used to achieve neuronal-specific labelling. The rAAV-hSYN-Cre with serotype 1/2 drives Cre expression in neurons around the injection area (radius ca. 2 mm). rAAV-hSYN-Venus was applied as a control virus. From here on, Serotype 1/2 rAAV-hSYN-Cre virus is referred to as rAAV-Cre and rAAV-hSYN-Venus as rAAV-Venus. The rAAV-Cre virus (diluted 1:5, 1:10 or 1:20 in PBS) or a control (PBS or rAAV-Venus (1:5 in PBS)) was delivered to the brain's hippocampal region of 3 to 6-month-old loxP-mini*Tdg* mice by stereotactic injections using a glass capillary (BLAUBRAND® intraMark BR708707). Prior to injection, animals were deeply anaesthetized (isoflurane 1,5-2%, oxygen 2%), and general (Temgesic 0,03mg/ml and Metacam 0,5mg/ml) and local (Marcain 0,04ml/20g) analgesics were intraperitoneally and subcutaneously administered correspondingly. Anaesthesia was upheld throughout surgery by continuously administering isoflurane. Toe pinching and breathing rate were monitored to control anaesthesia depth. Cranial boreholes were drilled following stereotactic coordinates set relative to the bregma at Anterior-Posterior (AP) 2.0 mm from bregma, Medial - Lateral (ML) ±1.5 mm from the midline and Dorsal – Ventral (DV) 1.2 mm (the first injection site, 210 nl of 1:5 diluted virus) and 1.5 mm (the second injection site, 210 nl of 1:5 diluted virus) from the dura. After injections, animals were put back in their home cage and monitored until awake and presenting normal behaviour. Following behavioural analysis, Cre-induced GFP expression was assessed post-mortem by immunohistochemistry (IHC).

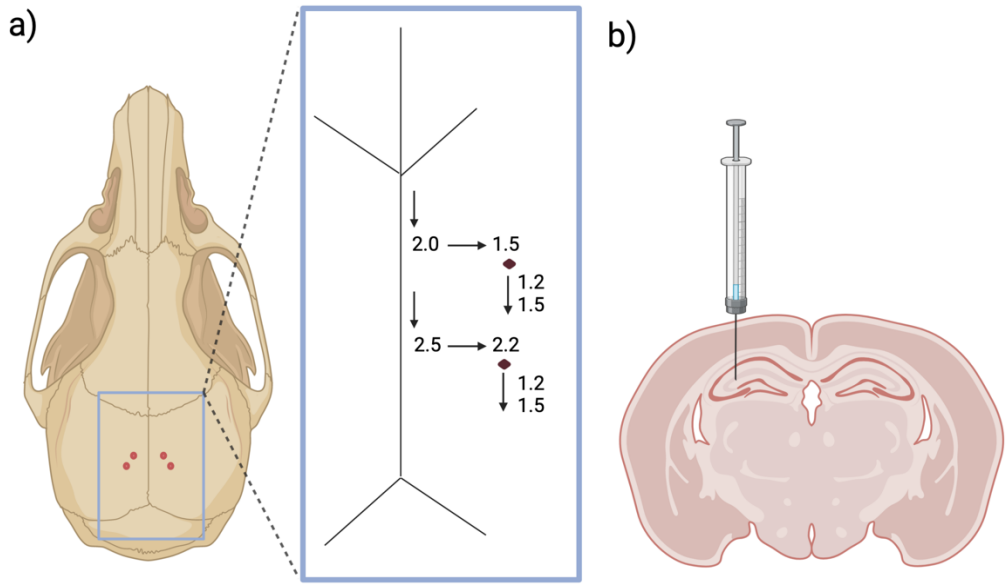

Figure 5. Stereotactic coordinates for surgical boreholes and viral injection.

a)Figure shows cranial boreholes and coordinates relative to bregma at AP 2.0 mm/2.5mm and Lateral 1.5mm/2.2mm, and injection depth at DV 1.2 and 1.5mm, here illustrated at the right hemisphere. b) Image show a section of the hippocampus illustrating the injection targeting DG and CA. Figure created in Biorender.

2.5 Behavioural studies

Spatial memory performance and behaviour of adult mice with rAAV-Cre-induced hippocampal-specific TDG deletion was assessed. Behaviour studies were performed using 3-6 month-old male mice. Prior to habituation and testing, animals were accustomed to being handled by the experimenter once a day for three days, lifting each mouse repeatedly by its tail for 3-5 minutes to avoid novelty-induced stress. The video-tracking system ANY-Maze recorded animal movement from above in all tests. All fields were cleaned with soap water between each trial to minimise olfactory cues.

2.5.1 Open field Test (OFT)

The open-field test (OFT) consists of a white square open field box (LxWxH 50x50x30) with a proximal cue attached to one of its walls (Figure 6a). Mice were placed in the field facing the corner closest to the experimenter and allowed to explore the field for 10 minutes before returning to their home cage. Using the ANY-maze software analysis package, a series of 16 squares were determined and used to evaluate subject tracks. The squares were then group together as zones: centre, side and corner (figure 6a).

2.5.2 Novel Object Location (NOL) task

Following a modified, published protocol [94], long-term memory of a spatial location was tested by the novel object location (NOL) test. NOL habituation and testing were performed in the same field as for the OFT, with the addition of two identical objects placed 12,5 cm from the arena walls and 25cm away from each other (figure 6b). The

objects chosen had a smooth surface and a height of approximately 10 cm, so animals could not climb them. Mice received three exposure trainings for 10 minutes, with two identical objects placed next to each other. For the test day (10 min), one of the objects is moved to a new location (diagonally opposite). Training sessions and test is given with an intertrial interval of 24h. The novelty preference is assessed by object-sniffing episodes and the time spent near the object. A maximum exploration time of 30 seconds is given. If the animal spends a combined amount of 30 seconds exploring the objects, the test will stop. If the animal does not explore the objects for 30 seconds, the test will stop after 10 minutes. After each habituation and trial session, objects and the arena were cleaned with soap water to minimise olfactory cues.

2.5.3 Y-maze test

The Y-maze (figure 6c) consists of three identical sections forming a Y-shape (LxWxH 35x7x15). The maze is elevated on a table with surrounding distal cues on the wall. Following a modified, published protocol [95], long-term memory of a spatial location was tested. During habituation, mice were allowed exploration in two of the arms of the Y-maze while the third arm was closed off. Habituation was done for 5 minutes each day for six consecutive days, with an intertrial interval of 24h. At the novelty preference test (day seven), the closed-off arm was opened, enabling the animal to explore the whole maze freely (figure 6c). The novelty preference is assessed by the time animal spends in the novel arm. Mice were always released in the bottom stem of the Y-maze. After each habituation and test session, objects and the arena were cleaned with soap water to minimise olfactory cues.

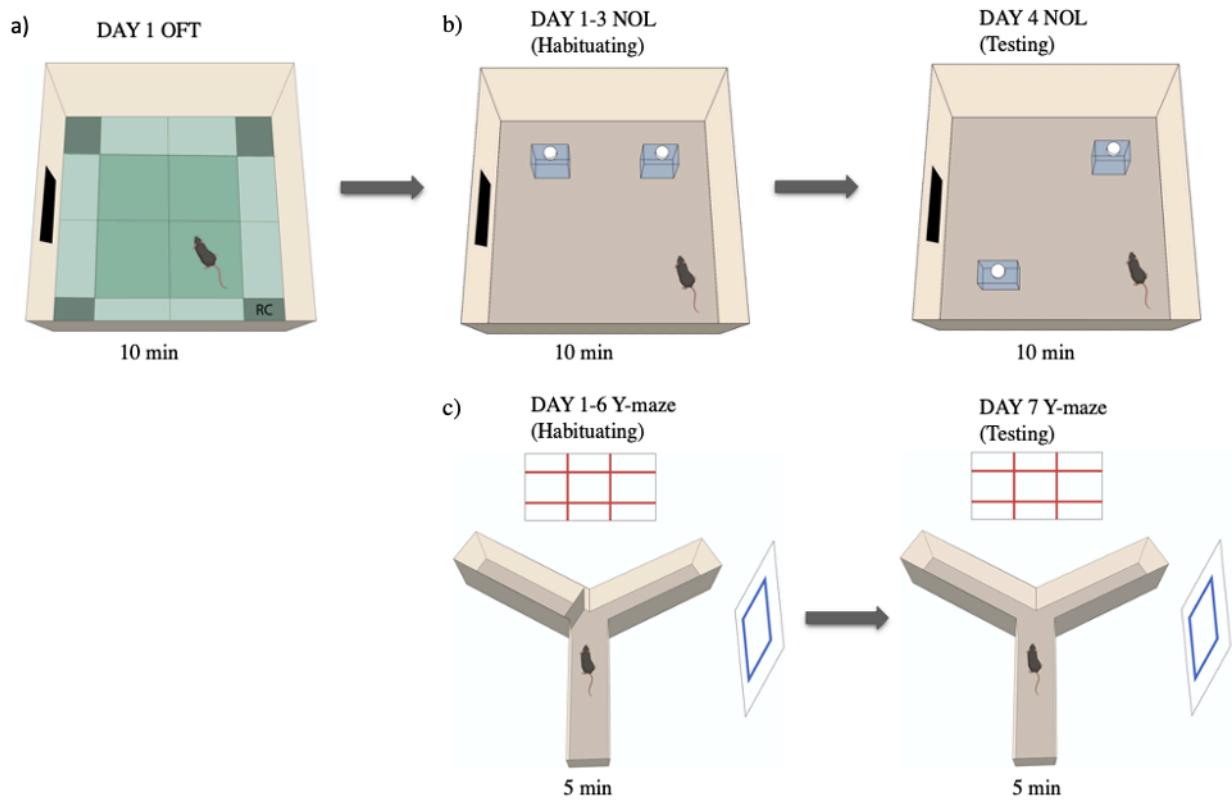

Figure 6. Experimental design for spatial reference memory and behaviour studies.

a) Open field arena depicts a series of zones used to identify subject tracks identified by the ANY-maze software analysis package. Corner, side and centre zones are represented in dark green, light green and green, respectively. A black visual cue card is indicated on the left side of the wall. b) NOL test arena shows the position of objects during habituation and testing, respectively. A black visual cue card is indicated on the left side of the wall. c) Y-maze test arena illustrates a closed-off left arm during habituation and an open left arm during testing. Different shaped and coloured visual cue cards are depicted on the arena´s walls. The figure was created using Rhino6/3d and Adobe Illustrator.

2.6 Perfusion

Animals were perfused 24h after the last behavioural test day (Y-maze day 7). Animals were anaesthetised by isoflurane and subsequently intraperitoneally injected with a lethal dose (2g/kg) of pentobarbital. Evaluating the paw and tail pain reflexes upon stimulation was used to indicate appropriate anaesthesia depth. Perfusion took place by making a thoracic incision opening the anterior chest wall, and exposing the sternum. The sternum and surrounding ribcage were cut to create an open chest cavity exposing the heart. With an 18G needle connected to a three-way stopcock (Braun), 0.9% saline solution was injected into the heart's left ventricle after clamping of the descending aorta and puncturing of the right atrium. Approximately 50mL saline solution was slowly injected to replace all blood through the blood circulation circuit.

2.7 Frozen sectioning

Following perfusion, the brain was carefully collected from the cranium by removing the occipital skin, cervical muscles and cranial bones. The right hemisphere was fixed in 4% paraformaldehyde (PFA) in PBS for at least 48h before being frozen with aerosol freezing spray (PRF 101/502 ML GREEN NFL). The brain was further cut into tissue sections with a thickness of 30µm using a cryostat (CryoStar NX40, Thermo Fischer, chamber and object temperature at -20°C). Sections were stored in 1x PBS with 3µl/10ml ProClin™300 (Sigma-Aldrich) in 1x PBS at 4°C. The left hemisphere was microdissected into sub hippocampal regions CA1, CA3 and DG and stored at -80° for later use.

2.8 Immunohistochemistry

Immunohistochemistry was performed on selected frozen sections (30µm) to visualise TDG-depleted GFP expressing cells in the hippocampal subregions CA1, CA3 and DG. Antigen retrieval was performed to reverse the antigen-masking effect caused by the formaldehyde fixation. This was done by incubating brain sections at 99°C for 3 min in 40mM of a pH 6 trisodium citrate solution (Trisodium citrate 5,5 hydrate (Merck-Millipore 1.06431.1000). Tissue sections were left to cool in solution for 27 min (total time in solution 30 min) at room temperature (RT) and washed 3x5 min in 1xPBS. After blocking unspecific binding sites with blocking buffer (5%NGS/5%BSA/0,1% Triton X-100 in PBS) for 2 hours at RT, sections were incubated with primary antibody solution (see Appendix table 2 for details on antibody solutions) overnight at 4°C while constantly shaken at 15 oscillations/min. Following washing for 3x (10-20-30 min) in PBS-T (PBS + 0,1% Tween20), sections were incubated in secondary antibodies (see Appendix table 3 for details on antibody solutions) in the dark for 2h at RT while constantly shaken at 15 oscillations/min. Sections were further washed 3x (10-20-30 min) in PBS-T (PBS + 0,1% Tween20). Tissue sections were mounted onto coated slides (ThermoFisher SuperFrost Plus) and left to dry overnight in a light protected container before being dipped into DAPI-solution (1:5000 in 1xPBS) for 1 min and washed 2 x 1x PBS and 1x ddH2O. Covers slips were placed after sections had dried using mounting oil (ProLong Gold Antifade Mountant with DAPI, Invitrogen, USA).

2.9 Zeizz Axioscan and confocal imaging

In this project, Zeiss® Axioscan and confocal imaging were performed to observe fluorescence in IHC stained brain sections. Imaging was performed using the whole slide scanner Zeiss® Axioscan Z1 (Zeiss;Jena; Germany) and the confocal laser scanning microscope Zeiss® LSM 800. For Zeiss® axioscan imaging, a Plan-Apochromat 20X/0.8 M27 objective was used. A single-focus layer without z-stacking was applied in the tissue detection and scanning process. To obtain the best image for each section, focus strategy settings were optimised individually. For imagining DAPI (AF405), the LED module Light source was set at 365nm. The light intensity settings were set at 20.90%, with an exposure time of 20,01 ms. For imaging of NeuN (AF647), the LED module light source was set at 625nm. The light intensity settings were set at 30%, with an exposure time of 75 ms. For imaging of GFP (AF488), the LED module light source was set at 470nm. The light intensity settings were set at 40%, with an exposure time of 30 ms. For confocal

imagining, a Plan-Apochromat 40X/NA oil emersion objective was used. The pinhole, gain and intensity used were selected depending on the excitation and emission spectra of each fluorescent protein or antibody (GFP, GFAP and NeuN). Z-stack height was adjusted for each sample using the channel for neuronal marker NeuN to determine section depth. All images were processed using Zen software (Zeiss).

2.10 Statistical analysis

Collected data from behavioural tests were subjected to statistical analysis using the software GraphPad Prism (version 9.3.1). Animals were grouped based on the type of injection received (rAAV-Venus, PBS or rAAV-Cre (diluted 1:5, 1.10, 1:20)) or not receiving an injection at all (Naïve). A ROUT test was applied to find any number of outliers. A one-way ANOVA and t-test was used for comparison between groups. A two way-ANOVA was performed to assess the significance between groups and performance. A Tukey's test was used for the correction of pairwise comparisons. A non-parametric One-sample t-test was done to determine whether performance differed significantly from the chance performance (15 sec or 50%). Statistical significance was considered at a probability level of 95%.

3 Results

3.1 rAAV-induced TDG depletion in hippocampal neurons

We used an rAAV carrying the hSYN promoter to achieve neuron-specific labelling. The serotype 1/2 rAAV-Cre drives Cre expression in neurons around the injection site. By introducing Cre expression, the LoxP-flanked *Tdg* and the STOP signal before eGFP is deleted (figure 3). This allows us to visualize TDG depletion by eGFP signal after IHC. PBS and rAAV-Venus was applied as a control. A total of 47 mice were injected with different concentrations of rAAV-Cre virus (20x 1:5, 2x 1:10, 7x1:20) or a control (11x PBS and 7x rAAV-Venus (1:5)).

3.1.1 Improving the injection coordinates to target viral infection in the whole hippocampus

For the first trials of virus injection, I followed stereotactic coordinates AP 2.0 mm from bregma, ML ±1.5 mm from the midline and DV 1.2 mm (the first injection site, 210 nl of 1:5 diluted virus) and 1.5 mm (the second injection site, 210 nl of 1:5 diluted virus) from the dura. A total of 420nl of the rAAV-Cre virus were injected in the hippocampal region of both hemispheres. IHC analysis was performed to assess the rAAV-Cre-induced GFP expression. In this case, we found that GFP expression was mainly restricted in CA3, and almost no GFP signals were observed in CA1 and DG neurons, as exemplified by TDG_247 shown in figure 7. In some cases, such as TDG_313 (figure 7), a GFP expression was mainly detected in the DG, suggesting a more ventral injection. To target viral infection in the whole HPC, we improved our protocol for virus injection. 1) In addition to the previous injection site at AP2.0/ML±1.5, a second injection site at AP 2.5/ML±2.2 was introduced. 2) The volume of virus ijected at each site was reduced from the previous 210nl to 105nl. 3) Different DV coordinates were tested, e.g., the first injection site at DV1.1 or DV1.2 and the second injection site at DV1.5 or DV1.8. After optimizing the viral injection protocol, we found that the addition of an injection site at AP2.5/ML±2.2 improved the spread of viral infection in the whole HPC, such as seen for TDG_360 shown in figure 7. We found that injection at DV 1.5 and DV1.8 both resulted in GFP expression in DG, such as for TDG_313 (DV 1.2 and 1.5) and TDG_360 (DV 1.2 and 1.8) (Figure 7). Both injections at DV1.1 or DV1.2 showed a GFP signal covering CA1. Therefore, I conclude that the injection coordinates: (AP 2.0mm and 2.5 mm, ML 1.5 mm and 2.2 mm, and DV 1.2 and 1.8 mm) are optimal to achieve a more even distributed viral infection in the whole HPC (*TDG_360, Figure 7).*

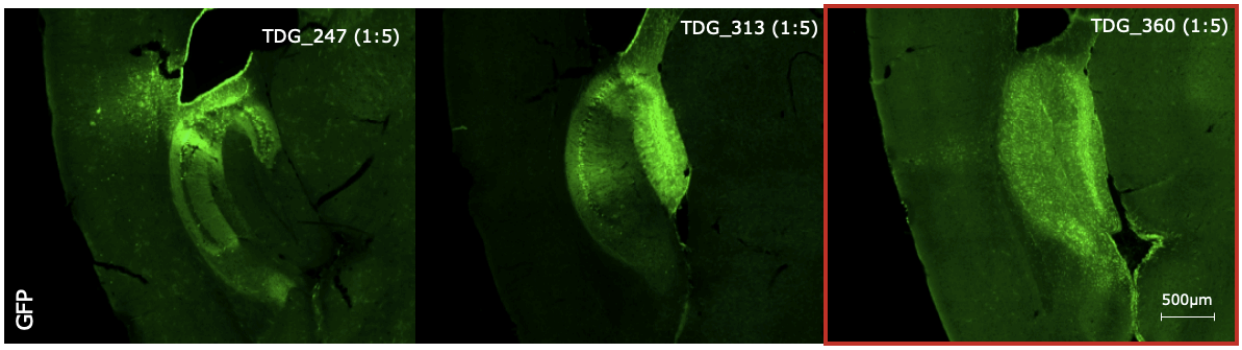

Figure 7. Improving injection site targeting hippocampal CA and DG.

The images show GFP stained hippocampal region (30µm brain section, Axioscan from Zeiss). Green fluorescence indicates the infection of rAAV-Cre around the local injection site. Three representative images show the Cre-induced GFP expression in three loxP-miniTdg mice, e.g., TDG_247 displays a more lateral injection, therefore only targeting CA3, not covering CA1 and DG. TDG_313 shows a more ventral injection mainly expressed in DG. TDG_360 shows distributed infection of rAAV-Cre in the whole HPC after optimising injection coordinates (AP 2.0mm and 2.5 mm, ML 1.5 mm and 2.2 mm, and DV 1.2 and 1.8 mm). IHC was performed by Konstanse Skogøy Innvær. Images was processed in Zen software (Zeiss).

3.1.2 Improving injection procedure to minimise infections and tissue lesions due to the surgery procedure

Staining for Glial Fibrillary Acidic Protein (GFAP) was performed to assess infection caused by the surgery procedure. GFAP is a common biomarker for astrocytic cells in the central nervous system (CNS). A major function of astrocytes involves their activation in response to damage, including trauma, infection and neurodegeneration [96]. Normally, astrocytes are found in a quiescent state in the CNS. When activated, astrocytes express high levels of GFAP and display morphological changes such as synaptic elongation and an increase in cell mass and number [96] [97]. Thus, IHC of GFAP allows us to visualise an active immune response to infection. For the first trials of injections, we detected an immune response in PBS-injected animals by IHC of GFAP, showing activated astrocytes, which may be due to infections contracted during the surgery procedure per se. Such as for TDG_330 (Figure 8), high levels of GFAP and synaptic elongation are observed after PBS injection. Cell mass and number are also increased as compared to non-injected animals, such as TDG_275 Naïve (figure 8). TDG_275 (Naïve) show normal distribution of quiescent astrocytes, suggesting no immune response. To minimise the infection during surgery, I made the following improvements: 1) Instead of drilling a hole through the cranium, a thin layer of bone was left. A hole was poked through the remaining layer with a small needle, opening for insertion of the glass capillary. A smaller borehole minimises the chance of infection during the surgery. 2) The glass capillary and virus were administered slowly with great care to avoid tissue lesions. 3) With the addition of a second injection site, the volume injected at each site was smaller. This minimises the risk of lesions caused by the physical pressure of injecting a fluid into the brain. After optimising the surgery procedure, we barely detected any activated astrocytes by GFAP staining, as seen in control injected animals exemplified in figure 9 TDG_365 section 3.1.3.

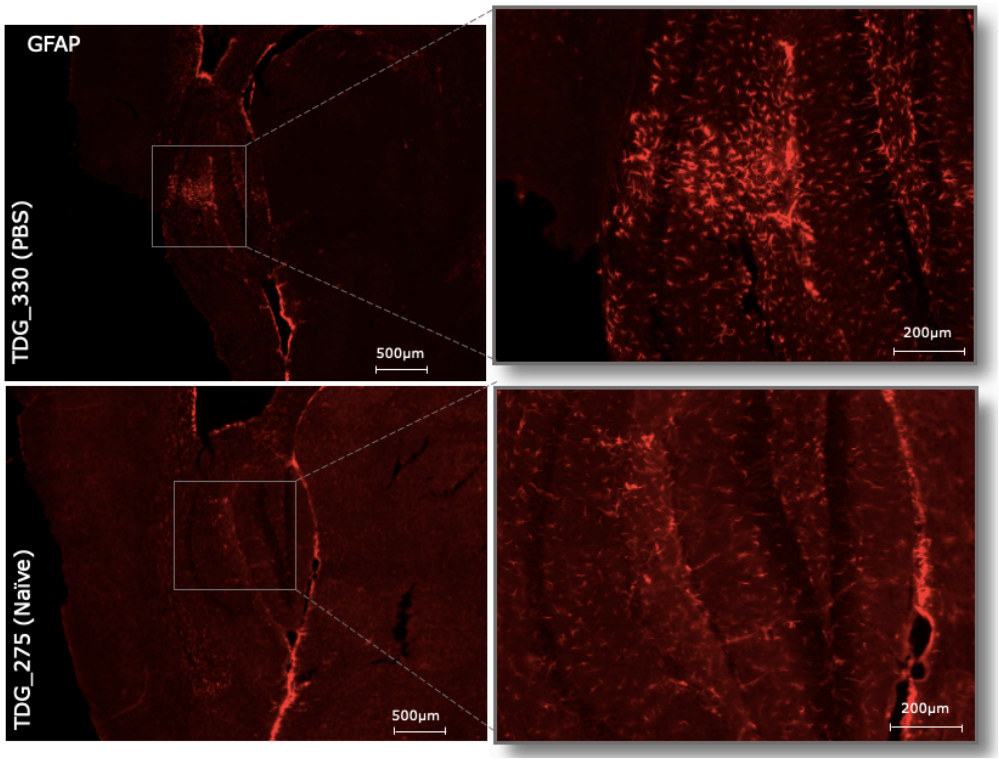

Figure 8. IHC of GFAP showing activation of astrocytes in PBS injected and Naïve animals.

Two representative images show GFAP stained hippocampal regions (30µm, Axioscan from Zeiss) in two loxP-miniTdg mice; one injected with PBS (TDG_330) and one Naïve (TDG_275). GFAP-positive astrocytes are shown in red. TDG_330 (PBS) show some astrocytic activation, as detected by synaptic elongation and an increase in cell mass. TDG_275 (Naïve) has not received any injection and shows no astrocytic activation, as detected by low expression of GFAP. IHC performed by Konstanse Skogøy Innvær. Images processed in Zen software (Zeiss).

3.1.3 Reducing Cre-induced neuronal loss and tissue lesions by an optimised viral titer

Staining for the nuclear antigen NeuN was performed to evaluate healthy neurons in the brain after viral injection. NeuN is commonly used as a biomarker for neurons, and neuronal health can be evaluated by detecting regular NeuN expression [98]. This allows us to visualise neuronal loss and tissue damage by IHC. For the first trials of virus injections (concentration of 1:5), severe neuronal loss was observed around the injection site, as seen in figure 9a TDG_360. Additionally, strong activation of astrocytes was detected by IHC of GFAP, indicating an immune response (figure 9a, TDG_360). Animals injected with PBS or control virus (rAAV-venus) show healthy hippocampal neurons without any lesions, as exemplified by TDG_356 in Figure 9a (see Appendix figure 15. for more NeuN staining of PBS, rAAV-Venus control and Naïve animals showing no lesions). Animals injected with rAAV-Venus show no GFP expression. Venus is a YFP protein and could be visualized using the anti-GFP antibody, explaining the fluorescent signal detected in rAAV-Venus injected animals (figure 9a, TDG_356). Similarly,for non-injected animals (Naïve), no immune response was observed in mice injected with control (rAAV-Venus), as shown by GFAP-positive quiescent astrocytes. These observations indicate that neuronal loss, tissue lesions and astrocytic activation were induced by massive Cre-

expression, and not by the virus administration or surgery procedure. To solve this issue, we tested several viral dilutions to achieve minimal Cre-induced neuronal loss and the best viral infection efficiency. With a 1:5 viral dilution, Cre-induced GFP expression was high in CA1, along with severe neuronal loss and tissue lesions, as exemplified by TDG_258 (1:5) as shown in figure 9b. With a 1:10 viral dilution, again, severe neuronal loss and tissue lesions were observed in the CA1 region with strong GFP expression, such as TDG_178 (1:10), as shown in figure 9b. With a 1:20 viral dilution, Cre-induced GFP was evenly expressed in CA1 and DG without severe neuronal loss such as TDG_458 (1:20), as shown in figure 9b.

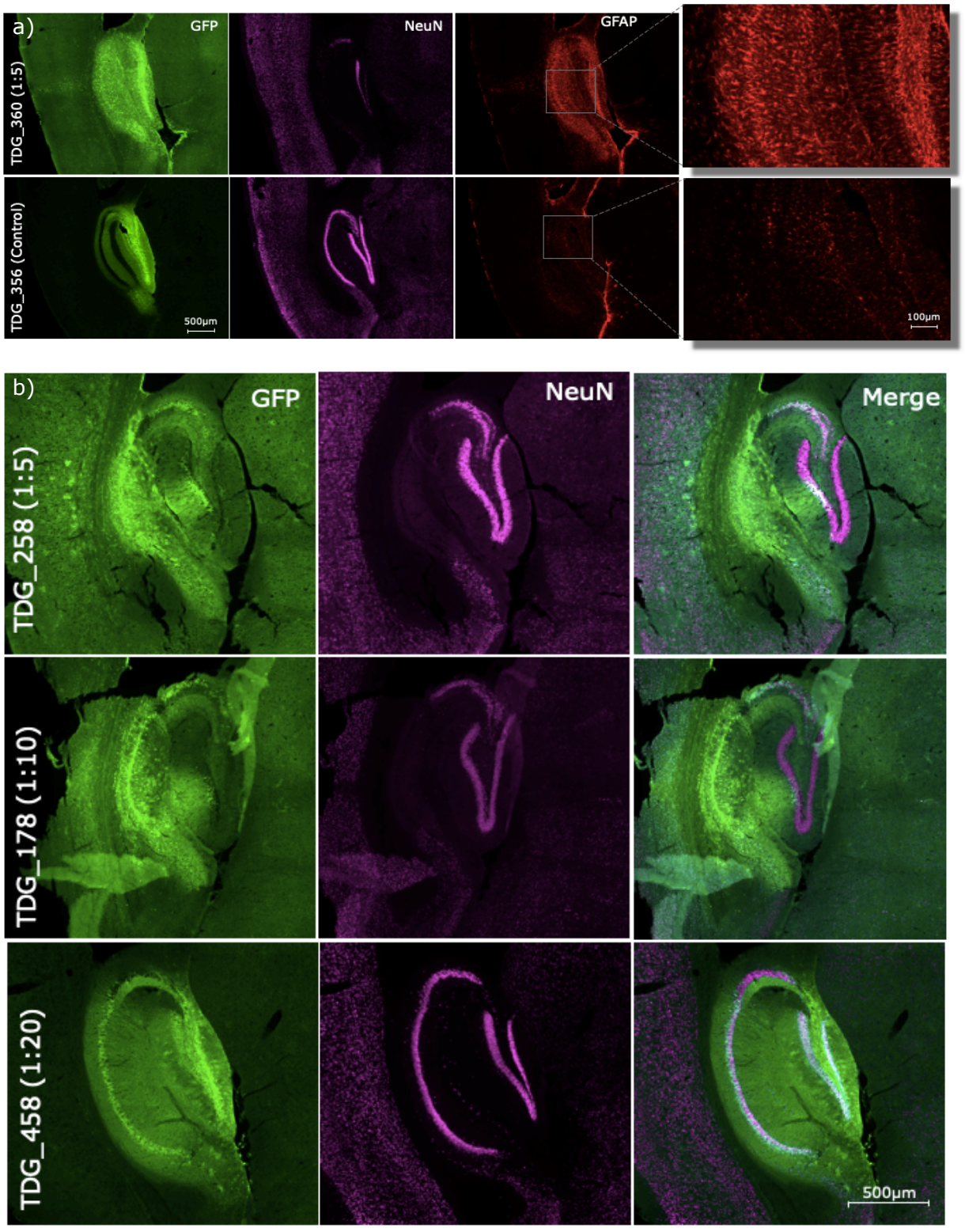

Figure 9. Cre induced GFP expression, neuronal loss and GAPH expression following rAAV-Cre injection.

IHC of GFAP shows activated astrocytes in Virus injected animals. The image show GFP (green), NeuN (Magenta) and GFAP (red) stained hippocampal regions (30µm, Axiosxab from Zeiss). a) Two representative images show activated astrocytes in the loxP-miniTdg mouse with an injection of rAAV-Cre (1:5) and quiescent astrocytes in the loxP-miniTdg mouse with an injection of rAAV-Venus control virus (1:5). b) Three representative images show GFP expression, neuronal loss and tissue lesions following the injection of rAAV-Cre with different concentrations (1:5, 1:10, 1:20).

Green fluorescence indicates the infection of rAAV-Cre around local injections. NeuN positive cells are shown in magenta. Staining performed by Konsanse Skogøy Innvær. Images processed in Zen software (Zeiss).

3.2 Assessing anxiety and long-term spatial memory of loxP-mini*Tdg* mice by behavioural studies

Behavioural studies were conducted to investigate whether depletion of TDG in the HPC affects anxiety-related behaviour and spatial memory in mice. A total of 42 loxP-mini*Tdg* 4-6 month-old male mice were tested. Animals were grouped: 22x rAAV-Cre virus injected, 5x rAAV-Venus injected, 12x PBS injected and 4x naïve. Anxiety-related behaviour was examined in an open field test by measuring time spent in the corner and centre zone. We used two novelty preference tests (NOL and Y-maze) to investigate long-term spatial memory, giving animals a simultaneous choice between a familiar and novel spatial location. Animals not completing a test (Not exploring any objects before 10 min passed in NOL), or other difficulties (e.g. computer malfunction), led us to remove four animals before statistical analysis. All dependent variables fulfil relevant test assumptions (e.g. normal distributed). Mean (M) and standard deviation (SD) is given for all tests.

3.2.1 Open Field test

The open-field test allows us to measure exploration activity and anxiety levels of mice by examining movement and time spent in different regions of the novel open field, such as the side, corner, or the open, exposed centre zone. A decreased level of anxiety leads to increased exploratory behaviour (e.g. spending more time in the open, exposed centre zone) [99]. Hence, longer time recorded in the centre zone indicates reduced anxiety-related behaviour.

As shown in Figure 10a, Naïve loxP-mini*Tdg* mice and those with PBS injection spend similar time in the centre zone (Naïve: M=172 sec, SD=18.7, PBS: M=158 sec, SD=74,3). rAAV-Venus injected animals spent more time in centre (M=233 sec, SD=69.3) then in corner (M=121 sec, SD=43). This difference was significant (p = .006, two-way ANOVA), suggesting that these animals were less anxious. However, in mice with an injection of rAAV-Cre, a significantly less time spent in the centre (M=132, SD=30) compared to corner (M=194 sec, SD=26) was detected (p = .001, two-way ANOVA). This suggests that these animals are more anxious. Interestingly, mice with an injection of rAAV-Cre spent significantly less time in the centre zone than those injected with rAAV-Venus control viruses (rAAV-Cre: M=132 sec, SD=30, rAAV-Venus: M=233 sec, SD=69.3). This difference was significant (p = .001, Two-way ANOVA).

As described in section 3.1, most mice in the initial injection experiments show tissue lesions and/or activated immune cells in the HPC around the injection site, which might influence animal behaviour (Figure 9). Therefore, after surgery optimisation, I also analysed a select group of animals (n=4 naïve, n=5 injected with 1:20 rAAV-Cre), which showed healthy hippocampal tissues around the injection site (figure 10b). In this case, rAAV-Cre-injected animals still spend significantly less time in the centre (M=130, SD=27.1) then corner (M=188, SD=14.2). This difference was significant (p = .007,

Two-way ANOVA). This result suggests that mice with an injection of the rAAV-Cre show an increased level of anxiety.

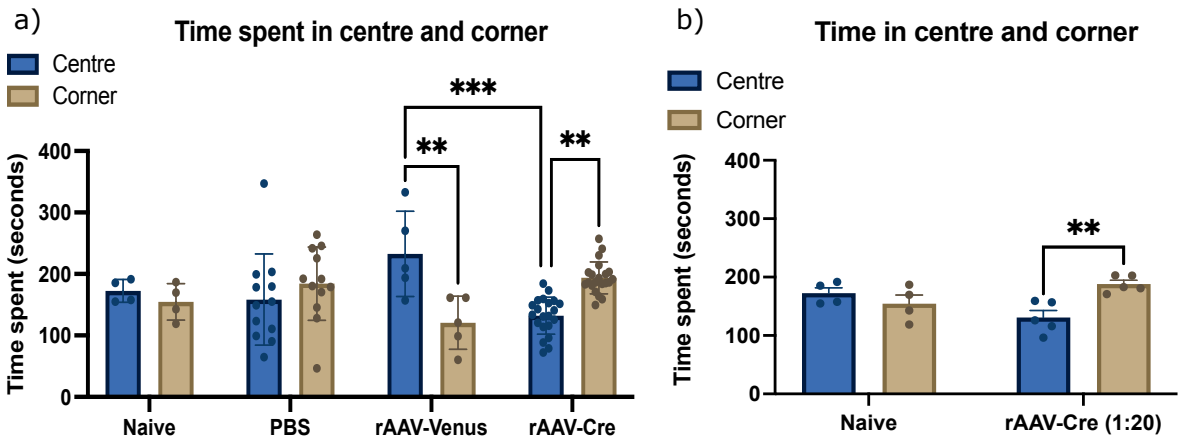

Figure 10. Time spent in centre and corner in an OFT for Naïve, PBS, rAAV-Venus and rAAV-Cre injected mice.

Coloured dots represent individual mice. a) The graph show performance for all animals: n = 4 naïve, 12 PBS, 5 rAAV-Venus and 21 rAAV-Cre mice. Significant differences in time spent in the centre and corner can be detected for rAAV-Venus control mice (p = .006) and rAAv-Cre virus mice (p = .001), Two way ANOVA. A significant difference in time spent in the centre can be detected between rAAV-Venus and rAAV-Cre injected animals (p = .001), Two-way ANOVA. B) The graph show performance of selected animals n= 4 Naïve, 5 rAAV-Cre (1:20) mice. Significant differences in time spent in the centre and the corner can be detected for rAAV-Cre (1:20) mice (p = .007, two-way ANOVA). Graphs created in GraphPad Prism.

3.2.2 Novel object location test

Normal mice preferentially explore a novel location over a familiar location. We investigated long-term spatial memory by the NOL test. The NOL test primarily evaluates spatial learning and memory by assessing preference for a novel spatial location. Mice received three 10-min exposure training trials in an open field with two identical objects placed next to each other. After exposure training, animals received a novel location preference test in which one of the objects was moved to a new location. The number of object-sniffing episodes and time spent near the object was recorded during the test. A maximum exploration time of 30 seconds was given. If the animal spent a combined amount of 30 seconds exploring the objects, the test was stopped. If the animal do not explore the objects for 30 seconds, the test was stopped after 10 minutes. A 24h intertrial interval separated the exposure and novelty location preference tests. With a 24h intertrial interval, short-term memory should have decayed, and performance should be reliant on long-term memory.

As shown in Figure 11, Naïve loxP-mini*Tdg* mice spend significantly more time exploring the novel object location (*M*=20.8 sec, *SD*=2.67) above the chance level (15 sec) (p = .023, one-sample t-test), suggesting that these animals have normal spatial memory. There is no preference for the novel object location in mice with PBS (*M*=16.1, *SD*=6.57) or rAAV-Venus control virus (*M*=10.2, *SD*=8.07) injection. However, mice with rAAV-Cre injection spend significantly more time exploring the novel object location (*M*=18.3, *SD*=4.06, p = .002, one-sample t-test). After surgery optimisation, I analysed a select

group of animals (n=4 naïve, n=5 injected with 1:20 rAAV-Cre) (Figure 11b). In this case, rAAV-Cre-injected animals show a significant preference for the novel object location above the chance level (M=20.8, SD=1.77, p = .002, one-sample t-test), suggesting normal long-term spatial memory. There is no significant differences detected between the groups analysed for NOL test (p = .115, one way-ANOVA, p = .997, t-test)

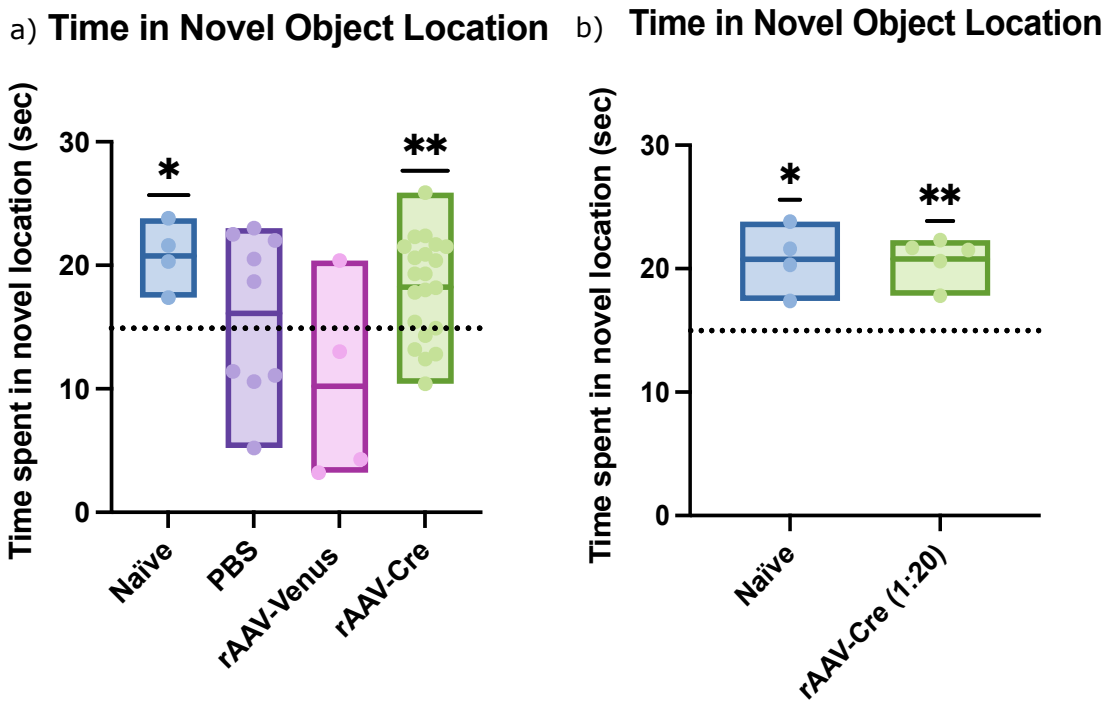

Figure 11. Time spent in novel object location for Naïve, PBS, rAAV-Venus and rAAV-Cre injected mice.

The dashed line indicates chance performance (15 sec). Coloured dots represent individual mice. A one sample t-test determines statistical significance. a) The graph show performance for all animals: n = 4 Naïve (p = .023), 12 PBS (NS), 5 rAAV-Venus (NS) and 21 rAAV-Cre mice (p = .002). b) The graph show performance of selected animals: n= 4 naïve (p=.023), 5 rAAV-Cre 1:20 (p=.002). Graphs created in GraphPad Prism.

3.2.3 Y-maze Test

LoxP-mini*Tdg* mice were tested for long-term memory of a spatial location by the Y-maze test. The test primarily evaluates spatial learning by assessing preference for a novel spatial location by using visual cues. Mice received six 5-min exposure training trials in two arms of a Y-shaped maze (stem and right arm). After exposure training, animals received a novelty preference test. They were allowed to explore the previously unvisited novel arm (left arm) and familiar arms (stem and right arm). The number of entries in each arm was recorded during the novelty preference test. A 24h intertrial interval separated the exposure training and novelty preference test.

As shown in figure 12a, Naïve loxP-mini*Tdg* mice (M= 61.3 %, SD=3.99) and those with PBS (M= 60.8 %, SD=7.01) and rAAV-Cre (M=60.1 %, SD=10.2) injection show a significant preference above chance (50%) to explore the novel arm (Naïve p =.011, PBS p < .001, rAAV-Cre p < .001, one-sample t-test). Although not significant, rAAV-Venus

control virus injected animals tend to prefer the novel arm (*M*=63.2, *SD*=13.4). As shown in Figure 12b, I analysed a select group of animals (n=4 naïve, n=5 injected with 1:20 rAAV-Cre) after surgery optimisation, which showed healthy hippocampal tissues around the injection site. In this case, rAAV-Cre-injected animals show no preference for the novel arm significantly above chance (*M*=55.5, *SD*=7.42). This random alteration between the novel and familiar arms suggests that animals injected with rAAV-Cre (1:20) have impairment in long-term spatial memory. There is no significant differences detected between the groups analysed for Y-maze test (p = .218 one way-ANOVA, p = .204 t-test).

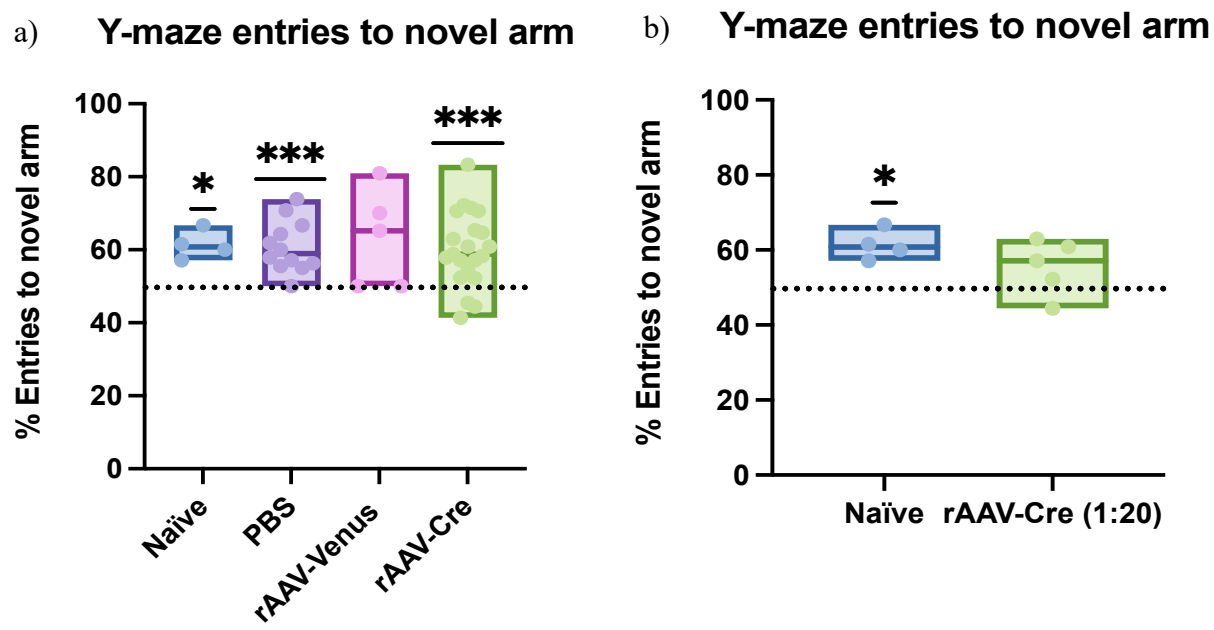

Figure 12. Percentage of entries to novel spatial location (novel arm y-maze) for Naïve, PBS, rAAV-Venus and rAAV-Cre injected animals.

The dashed line indicates chance performance (50%). Individual mice are represented by coloured dots. Statistical significance is determined by a one sample t-test. a) The graph show NOL performance for all animals: n = 4 Naïve (p =.011), 12 PBS (p < .001), 5 rAAV-Venus (NS) and 21 rAAV-Cre mice (p < .001). location b) The graph show NOL performance of selected animals: n= 4 naïve (p=.011), 5 rAAV-Cre 1:20 (NS). Graphs created in GraphPad Prism.

3.3 Tissue-and time-controlled deletion of TDG in a CamKIIα-Cre-miniTdg-ko mouse line

3.3.1 Establishing a brain-specific TDG depletion mouse model

To study the role of TDG in memory, independent of its role in development, spatially restricted excision of *Tdg* in adult neurons must be accomplished. We generated a neuron-specific *Tdg* knockout mouse model (CamKIIa-*Tdg*-ko) by crossing loxP-mini*Tdg* mice with a Tg(CamKIIa-Cre)T29 mouse strain (Jaxson lab).

To achieve this, I first crossed LoxP-mini*Tdg* (female) with Tg(CamKIIa-Cre)T29 (male) to produce heterozygous offspring. The genetic information in these offspring are Mini*Tdg*$^{+/-}$, WT *Tdg*$^{+/-}$, and CamKIIa-Cre$^{+/-}$, as shown in the breeding scheme in figure 13a. Secondly, I crossed heterozygous female mice (mini*Tdg*$^{+/-}$, WT *Tdg*$^{+/-}$ and CamKIIa-Cre$^{+/-}$) with male loxP-mini*Tdg* mice (mini*Tdg*$^{+/+}$, WT *Tdg*$^{-/-}$). This generated offspring with four different genotypes (group 1-4 figure 13a). The genetic information of the first group (1) is mini*Tdg*$^{+/+}$, WT *Tdg*$^{-/-}$ and CamIIa-Cre$^{+/-}$. The genotype is confirmed by PCR, as exemplified by animals numbered 5, 7 and 10 as shown in figure 13 b. Animals with this genotype are expect to have Cre mediated *Tdg* depletion. The genetic information of the second group are mini*Tdg*$^{+/+}$, WT *tdg*$^{+/-}$ and CamKIIa-Cre$^{+/-}$, confirmed by PCR as shown in figure 13b, numbers 4, 11, 12. The genetic information of the third group are mini*Tdg*$^{+/+}$, WT *Tdg*$^{+/-}$ and CamKIIa-Cre$^{-/-}$, confirmed by PCR as shown in figure 13b, number 6. The genetic information of the fourth group are mini*Tdg*$^{+/+}$, WT *Tdg*$^{-/-}$ and CamKIIa-Cre$^{-/-}$ confirmed by PCR, as shown in figure 13b, numbers 13 and 14. The fourth group can be used as control animals, as they have the same genotype as the original LoxP-mini*Tdg* animals.

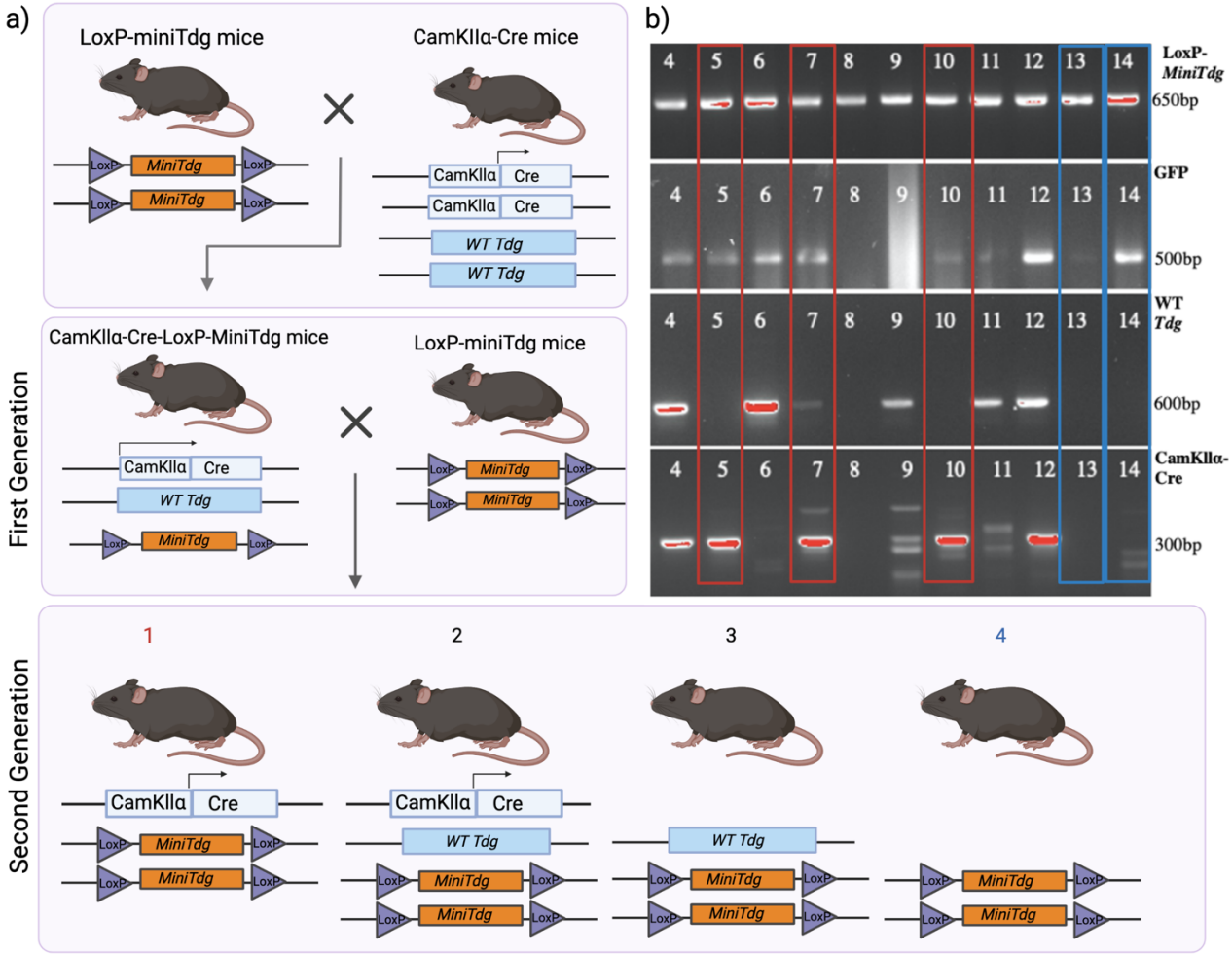

Figure 13. Generation of a neuron-specific *Tdg* knockout mice strain.

a)The figure shows the breeding scheme for generating a CamKIIα-Cre-miniTdg-ko strain. Mice homozygous for LoxP-miniTdg (female) are crossed with Tg(CamKIIα-Cre)T29 (male) to produce offspring with genotype MiniTdg$^{+/-}$, WT Tdg$^{+/-}$ and CamKIIα-Cre$^{+/-}$. For the second round of mating, female offspring from the first mating is crossed with LoxP-miniTdg $^{+/+}$ male mice. This generates offspring with four different genotypes (1-4 second generation). Approximately 25% of offspring

will have our desired genotype loxP-miniTdg$^{+/+}$, CamKIIα-Cre$^{+/+}$ and WT$^{-/-}$ (Group1). b) The image depicts a selection of gel electrophoresis results confirming genotype for second-generation offspring. The size of PCR products is indicated in bp. Figure created in Biorender.

3.3.2 Cre-induced *Tdg* KO and GFP expression in the CamKIIα-*Tdg*-KO mouse model

The CamKIIα promoter control Cre expression specifically in forebrain neurons, predominantly in the hippocampal CA1 pyramidal layer, starting from P20 and reaching the peak expression at P29 [88]. By introducing the expression of Cre recombinase, the loxP-flanked mini-*Tdg* as well as the STOP codon before eGFP is deleted. We collected brain samples from the CamKIIα-*Tdg*-KO mice at the postnatal day 40 (P40) and performed IHC using antibodies against GFP and NeuN. We found that Cre-induced GFP expression was predominantly in CA1 pyramidal neurons, as well as in a proportion of CA3 pyramidal neurons and DG granular neurons (figure 14). This result confirms that the newly established CamKIIα-*Tdg*-KO mouse model has neuron specific TDG depletion in the HPC.

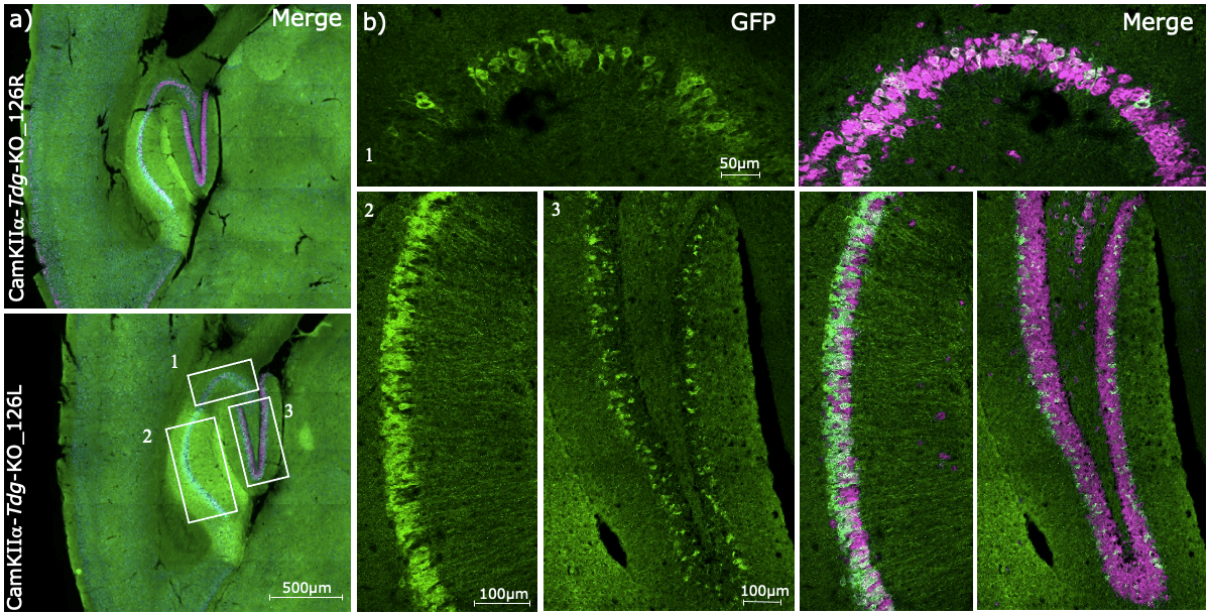

Figure 14. IHC of CamKIIa-*Tdg*-KO hippocampus at P40.

Green fluorescence indicates Cre-induced GFP expression. NeuN positive cells are shown in magenta. a) *Two images show GFP and NauN stained hippocampal region (30µm, Axioscan from Zeiss). Representative images show Cre-induced GFP expression and Neuronal health in both hemispheres of one* CamKIIa-*Tdg*-KO mouse (CamKIIa-*Tdg*-KO_126R and CamKIIa-*Tdg*-KO_126L). Hippocampal subregions CA1 (1), CA3 (2) and DG (3) are highlighted in the figure, respectively. b) *Three images show GFP and NauN stained hippocampal subregions (30µm confocal). Representative images show Cre-induced GFP expression in hippocampal neurons (left hemisphere* CamKIIa-*Tdg*-KO_126L*). Hippocampal subregions CA1, CA3 and DG are represented with numbers 1, 2 and 3, respectively. Images processed in* Zen software (Zeiss).

4 Discussion

4.1 rAAV-induced TDG depletion in hippocampal neurons

4.1.1 main findings

To study the role of TDG in memory, independent of its role in development, spatially restricted excision of *Tdg* in the hippocampus must be accomplished. We used a loxP-mini*Tdg* transgenic mouse model and optimised a protocol for rAAV-Cre induced TDG depletion in hippocampal neurons. We found that injection following stereotactic coordinates AP 2.0 mm and 2.5 mm, ML 1.5 mm and 2.2 mm, and DV 1.2 mm and 1.8 mm led to an even distribution of viral infection in the whole HPC. Also, we could reduce infection at the injection site by improving the surgery procedure. Furthermore, we found that a viral dilution of 1:20 reduces Cre-induced neuronal loss and tissue lesions while still giving a good viral infection efficiency. We observed that the immune response detected by activated GFAP was strongly reduced with a lower viral concentration. Conclusively, with a viral dilution of 1:20, we could have Cre-induced GFP expression and subsequent *Tdg* Knockout in all hippocampal subregions (CA1, CA3 and DG) and avoid neuronal loss, hippocampal tissue lesions and infection.

4.1.2 Critique of the methodology

A strength of using conditional gene knockout technologies is that one can deplete functionally essential genes in adult animals and circumvent difficulties associated with embryonic lethality. Additionally, one can achieve a time-and tissue-specific gene knockout. This gives a more accurate picture of gene function, as genes can have several purposes or expression patterns depending on the cell type or tissue. There are several advantages of using rAAV tools for Cre-induced *Tdg* depletion. First, the technique enables a local and specific knockout at the injection site. You can choose a precise location in the brain to deplete *Tdg*, as the conditional knockout is restricted to the area of viral spread. Secondly, the radius of infection is dependent on the viral titer, virus dilution, and the amount injected. All these parameters can be adjusted to accommodate the desired research objectives.

However, there are also limitations to using rAAv tools to induce *Tdg* depletion. First, the animal must undergo surgery to deliver the rAAV-Cre virus to the specific brain region. This can be stressful and straining for the animal. Secondly, the virus injection procedure is difficult to completely standardise, as there will be slight differences in the performance of the experimenter and individual differences in the animals. Third, the virus injection procedure is very time-consuming, and extensive training for the experimenter is needed. Lastly, we observe that Cre itself have properties causing tissue lesions and neuronal loss. This is a pervasive problem, as we observed that high concentrations of Cre cause not only gene knockout, but also neuronal loss and

hippocampal lesions. All these disadvantages will be discussed in relation to the obtained results.

4.1.3 Reliability and relevance of results

As depletion of *Tdg* using rAAV tools has previously not been attempted in our laboratory, a reliable method of injection had to be established. The first aim of this study was to successfully deplete TDG in the hippocampus. In this study, I found that optimal injection coordinates for targeting viral infection in the whole HPC were AP 2.0 mm and 2.5 mm, ML 1.5 mm and 2.2 mm, and DV 1.2 and 1.8 mm. However, even with the optimised injection coordinates, we observed some individual differences in spread of viral infection. This can be caused by several reasons: I) The surgery and virus injection constitute a demanding procedure, and there is a need for extensive training for the experimenter. The individual performance of the experimenter can vary to some degree, which can explain differences between injection quality, also in later stages after optimisation. II) The animals themselves have individual differences that can affect the procedure. For example, it can be challenging to correctly localise the hippocampus using the bregma as a visual cue, as the shape and size of bregma and the cranium vary from animal to animal. As a result, animals can receive an injection at an inaccurate location, causing some animals to only have *Tdg* depletion, e.g. at CA1, and others only in DG. Altogether, these complications can give unreliable results. Fortunately, successful viral infection and rAAV-Cre induced *Tdg* depletion can be assessed by IHC. By IHC of GFP, we can determine the efficiency of Cre-induced *Tdg* knockout by observing the number of cells emitting green fluorescent signals. By IHC of NeuN, we can assess the health and viability of neurons at the injection site. Thus, we can exclude animals that only have Cre-induced GFP expression, e.g. at CA3 or have severe lesions in the whole HPC. This allows us to remove animals with unsuccessful virus injections from the study, which increases the reliability of subsequent behavioural results.

Inflammation in the hippocampus has been linked to cognitive and emotional alterations in mice [100]. Therefore, as a second part of optimising, we tried to minimise infections in the brain due to the surgery procedure. In this study, we found that by decreasing the size of the cranial opening and by carefully administering the glass capillary, we could reduce astrocytic activation at the injection site.

A prevalent problem in this study was Cre-induced neuronal loss, tissue lesions and infection. We observed that Cre itself have properties causing neuronal loss and tissue lesions, as results from injection with rAAV-Venus and PBS did not show damaging effects. The Cre-loxP recombination system is a well-established tool for genetic manipulation, but research has suggested that this approach could also lead to adverse side effects [101]. Fordni et al. show that high levels of Cre recombinase expression in the nucleus of neuronal progenitor cells can compromise normal brain development in nestin Cre transgenic mice [102]. Further, Amin et al. report anatomical, neurochemical, and behavioural consequences in mice with rAAV-mediated Cre expression in the dopaminergic nuclei substantia nigra [103]. In this study, we observed severe neuronal loss and tissue lesions as a consequence of high concentrations of Cre. This is consistent with previous findings, stating that Cre has cell toxicity when expressed at high levels [104]. The toxic effects of Cre expression causing death in various cell types and tissues are presumably a consequence of Cre acting on LoxP-like sites present in the genome [105]. We also observed increased astrocytic activity with a high concentration of Cre.

This is presumably caused by an activated immune response as a reaction to Cre induced neuronal death. Altogether, this emphasises the need for careful control of Cre toxicity in the brain. Even though there are many disadvantages to using viral tools for *Tdg* knockout, many of these are circumvented by the optimised surgery procedure and controlling viral concentration. In future studies, the reproducibility of results will increase by using the optimised protocol and viral dilution together with extensive training for the experimenter.

4.2 Establishing a brain specific TDG depletion mouse model

To study the role of TDG in memory spatially restricted excision of *Tdg* in adult neurons must be accomplished. First, we depleted TDG with the use of viral tools. When using this technique, some difficulties were linked to the variation between individual animals and the reproducibility of successful results. Therefore, we wanted to generate a mouse line with conditional brain specific *Tdg* knockout. This can be achieved by having a tissue and time-specific promoter controlling Cre expression. The CamKIIα promoter control Cre expression specifically in forebrain neurons, predominantly in the hippocampal CA1 pyramidal layer, starting from P20 and reaching the peak expression at P29 [88]. By introducing the expression of Cre recombinase, the loxP-flanked mini-*Tdg* and the STOP codon before eGFP is deleted. In this way, we achieve a time-and tissue-specific *Tdg* knockout and evade difficulties associated with embryonic lethality.

4.2.1 Main findings

First, we generated a neuron-specific *Tdg* knockout mouse model (CamKIIα-*Tdg*-KO) by crossing loxP-mini*Tdg* mice with a Tg(CamKIIα-Cre)T29 mouse strain (Jaxson lab). Secondly, we confirmed that the newly established CamKIIα-*Tdg*-KO mouse model had neuron-specific TDG depletion in the hippocampus by IHC of GFP. We found that Cre-induced GFP expression was predominant in CA1 pyramidal neurons and a proportion of CA3 pyramidal neurons and DG granular neurons.

4.2.2 Critique of the methodology

There are several benefits of using a conditional knockout mouse model for TDG depletion. As previously established, by having a conditional knockout, we avoid difficulties associated with embryonic lethality. Further, many of the challenges we face when using viral tools for TDG depletion is avoided when using a conditional knockout mouse model. For example, there is no need for a surgical procedure that permits differences between individuals due to the procedure itself or the experimenter. Lastly, the CamKIIα promoter controlling Cre expression leads to a consistent distribution of Cre expression in neuronal cells, which gives higher reproducibility and reliability.

However, there are some disadvantages to the mouse model. First, creating the mouse model is time-consuming, and many animals are needed to facilitate this process. However, once generated, using these animals is less time consuming than performing individual injections in all animals to enable TDG depletion. Another weakness of the

mouse model is that the promoter used mainly causes expression in CA1 and less in CA3 and DG. Hence, we do not have an even TDG knockout in the whole HPC. Further, one cannot achieve the same location specificity as when using viral tools. With viral tools, one can choose exactly where in the brain to inject the virus and have a highly local Cre-induced TGD depletion. This will not be the case when a cell-specific promoter controls the expression. Further, the conditional knockout of loxP-mini*Tdg* is dependent on the specificity of the promoter controlling Cre expression. Sometimes, Cre expression is leaky, leading to widespread recombination. The Cre mouse line may occasionally delete floxed genes in the germline, in which the knockout allele may heritably remain in the offspring [106]. This must therefore be taken into consideration when generating a new conditional knockout mouse line.

4.2.3 Discussion of methodical approach and results

We generated a neuron-specific *Tdg* knockout mouse model (CamKIIα-*Tdg*-KO) by crossing loxP-mini*Tdg* mice with a Tg(CamKIIα-Cre)T29 mouse strain (Jaxson lab). I first crossed female mice homozygous for loxP-mini*Tdg* to a male Cre transgenic mouse (Tg(CamKIIα-Cre)T29) (Jaxson laboratory). Cre activity can vary depending on if the transgene is inherited from the male or female parent [107]. Floxed alleles can be converted to complete knockout if off-target issues cause Cre expression throughout the mouse. Choi et al. reported that when crossing CamKIIα-Cre mice with mice carrying a floxed LacZ reporter, the expression of lacZ is simultaneously induced by CamKIIα-Cre in the brain and testis [108]. Further, mating with mice that expressed LacZ in the male germ cells yielded offspring that expressed lacZ in the entire body [108]. Thus, the choice of sex for the Cre carrying mouse (Tg(CamKIIα-Cre)T29) must be considered. When generating a tissue-specific knockout, female Cre carriers have a genetically higher likelihood of expressing Cre in the germline, resulting in off-target expression. Therefore, we chose the male to be Cre carrier and breed to female floxed mice, as recommended by The Jaxson laboratory. In the second step of generating the CamKIIα-*Tdg*-KO strain, we crossed heterozygous female mice (mini$Tdg^{+/-}$, WT $Tdg^{+/-}$ and CamKIIα-$Cre^{+/-}$) with homozygous male loxP-mini*Tdg* mice (mini$Tdg^{+/+}$, WT $Tdg^{-/-}$). This generated offspring with four different genotypes. If any off-target issues cause Cre expression throughout the mouse, these animals will not develop beyond an embryonic state, as complete knockout of *Tdg* is embryonic lethal. In this way, offspring generated from the second generation mating presumably do not have any off-target issues. Approximately 25% of the progeny from this mating will be homozygous for the loxP-mini*Tdg* and heterozygous for the Cre transgene (mini$Tdg^{+/+}$, WT $Tdg^{-/-}$ and CamKIIα-$Cre^{+/-}$). These are our experimental mice. About 25% of the offspring will be homozygous for the loxP-mini*Tdg* but have no Cre transgene. These animals can be used as controls. The controls will not have Cre recombinase. Thus, any phenotypic differences between them and the CamKIIα-*Tdg*-KO mice should be due to the deleted gene in CamKIIα-*Tdg*-KO mice.

Previous literature shows that the CamKIIα promoter control Cre expression specifically in forebrain neurons, predominantly in the hippocampal CA1 pyramidal layer starting from P20 and reaching the peak expression at P29 [88]. To confirm that the newly established CamKIIα-*Tdg*-KO mouse model had neuron-specific TDG depletion in the hippocampus, we performed IHC of GFP at P40 CamKIIα-*Tdg*-KO mice. We expected prominent GFP expression in CA1 and some in CA3 and DG. Consistent with previous findings, Cre-induced GFP was predominantly expressed in CA1 pyramidal neurons, as observed with Zeiss Axioscan. When closer examining the hippocampal subregions CA3

and DG with confocal imaging, we observed expression in a proportion of CA3 pyramidal neurons and DG granular neurons. Some Cre-induced GFP expression was also observed in MEC. In future studies, we can determine the ratio of cells expressing GFP to total cells in CA1, CA3 and DG. Also, we can further assess Cre-Induced GFP expression in other brain regions. Further, these animals can be used in future behavioural studies to determine the role of TDG in hippocampal-dependent memory.

4.3 Assessing functional spatial memory after hippocampal *Tdg* depletion

Long-term memory is dependent on the transcriptional regulation of genes with important roles in memory formation [66]. The methylation landscape in part determines the transcription of these genes [9]. Thus, the regulators of the methylation pattern are essential for long-term memory formation through their role in transcriptional regulation. TDG's role in demethylation implicates a possible role of TDG in long-term memory formation. We hypothesised that the depletion of TDG should affect long-term memory, as this type of memory depends on transcriptional regulation. This follows the theory that short-term and long-term memory depends on different processes. Some genes are necessary for short-term memory of recently visited places, and others for the ability to form long-term associations between particular spatial locations [95]. We wanted to investigate TDG's role in long-term hippocampal-dependent memory through behavioural studies of mice with TDG depletion.

4.3.1 Main findings

The main aim in this study was to investigate whether depletion of TDG in the hippocampus affects behaviour and spatial memory. To achieve this, I examined mice with rAAV-cre induced hippocampal *Tdg* knockout in behavioural tests. My results show that animals injected with rAAV-Cre have increased anxiety-related behaviour. However, it is not clear whether depletion of TDG in hippocampal neurons affects the animal's long-term spatial memory. The animals involved in this study had different viral induced cre expression, issues of inflammation and neuronal loss.

4.3.2 Choice of behavioural tests

The NOL test is similar to the widely used novel object recognition (NOR) task. The NOL and NOR tests are practical behavioural tests commonly used to reveal the function and relative health of specific brain regions involved in memory [94]. While both tests exploit the inherent preference of mice for the novelty to reveal functional memory, the NOL test primarily evaluates spatial memory, which relies heavily on hippocampal activity [94]. Assessing spatial memory is dependent on the presence of spatial cues that the animals can use to orient themselves. On the other hand, the NOR test evaluates non-spatial learning of object identity, which relies on multiple brain regions [94]. We are depleting TDG specifically in the HPC and are interested in investigating TDG's role in hippocampal-dependent memory. Thus, the NOL test was a natural choice of test to answer our research question.

Typically, both the T-maze and Y-maze are used to assess working memory by evaluating the ability of mice to distinguish between a previously visited arm or a novel arm [109]. When assessing working memory, the arms of the mazes contain a reward. The Y-maze test used in this study was constructed to assesses spatial memory by including spatial cues that the animals can use to orient themselves. Spatial memory is evaluated by exploiting the inherent preference of mice for novelty. The animal is exposed to a familiar (already explored arm) and a novel arm. A mouse with intact spatial memory will remember the arms previously visited and show a tendency to enter the novel arm [110]. Both the T-maze and Y-maze can be utilised for assessing working memory and spatial memory. However, the Y-maze is sometimes preferred due to the more natural angels of the maze, making learning performance easier for mice.

4.3.3 Critique of the methodology

A strength of this study is the use of well-characterised behavioural tests used to assess anxious behaviour (OFT) and long-term spatial memory in mice (NOL and Y-maze) [111, 112]. These tests have been widely used for several reasons. 1) they are simple to conduct, and there is no need for extensive training for the experimenter. 2) There is no need for incentives or negative external reinforcement. 3) There is no need for food deprivation, and the tests are not associated with stress or pain for mice, as opposed to other behavioural tests such as Morris water maze or fear conditioning tests.

However, there are some weaknesses in this study. The OFT used in this study assesses anxiety by recording time spent in the centre compared to time spent in the corner. Notably, the test does not assess other possible indications of anxiety-related behaviour, such as defecation, shivering or gnawing on walls [113]. Thus, an animal can in theory spend a lot of time shivering in the centre, but this will not be recorded as anxious behaviour. The Y-maze and NOL test depends on the curiosity and willingness of a mouse to explore. Therefore, a weakness of these tests is anxiety-related behaviour in animals leading to less explorative behaviour [114]. To correct for this, the OFT is performed. Thus, animals displaying high anxiety levels in the OFT are taking into consideration when analysing results. In behavioural tests, use of reinforcements can be positive and negative. On one side, without e.g. negative reinforcements, there are no pain of fear induced for the animal. On the other side, tests using no reinforcements do not create a very strong memory. For example, in the NOL and Y-maze test, failing to explore an object is not penalised. However, receiving pain or fail to find food can be critical for a mice in its natural habitat [117]. Therefore, memory formed by having positive or negative reinforcement may affect the speed of learning and the strength of memory formed [117]. A general disadvantage for all the behavioural tests is the possibility of changes in external factors affecting the animal's behaviour [115]. This includes olfactory cues, auditory cues and visual cues. Deviations in such external stimuli can cause changes in behaviour, and thus the recorded behaviour can be incorrectly interpreted. Testing in a purpose-built behavioural test room shields the animals from these external factors. However, even under controlled conditions, environmental factors has some inevitable effects on behaviour (e.g. some olfactory and auditory cues from the handler that can differ between training days)[116].

4.3.4 Reliability and relevance of results

To our knowledge, behavioural studies on mice with hippocampal TDG depletion have previously not been conducted. Thus, there is no current literature to which my results can be compared. Therefore, I will mainly discuss the reliability and relevance of the results obtained in this study.

Reliability and relevance of results: OFT

In this study, we found that mice with an injection of the rAAV-Venus control virus spent significantly more time in the centre zone than in the corner. This suggests that these animals were less anxious. Our hypothesis expected that the mice injected rAAV-Venus control virus behaved similarly to Naïve and PBS injected animals, as none of these animals is affected by Cre-induced *Tdg* depletion. However, rAAV-Venus control injected animals tend to spend more time in the centre than both Naïve and PBS injected animals. A possible explanation for the differences in behaviour can be that Naive animals have not undergone surgy, as opposed to animals injected with PBS and rAAV-Venus control virus. Undergoing surgery can be stressful for the animal. The previous handling associated with the surgery, and possible hippocampal damage or infection, can explain the difference in behaviour. However, there are also contradicting results between the groups of PBS and rAAV-Venus injected animals. My results show that PBS injected animals tend to be more anxious than rAAV-Venus control virus injected animals. There are several possible explanations for this. I) The animals injected with PBS were the first to undergo the surgical procedure. Consequently, these animals received injections in an early stage of the study where the procedure's optimisation was not completed, and the experimenter had little training. Thus, these animals were subjected to a higher risk of hippocampal damage and infection due to the surgery. II) The sample size of the groups compared are different. Several more animals were injected with PBS than the rAAV-Venus control virus. In the early stages of the study, we did not have the proper control (rAAV-Venus). Therefore, we used PBS (as the rAAV-Cre virus we injected was diluted in PBS). III) There is great variance within the groups compared. The high variance within the group injected with PBS is due to larges differences within the surgical procedure in the early stages of training. Altogether, this could explain why rAAV-Venus control virus injected animals show a less anxious behaviour as compared to Naïve and PBS injected animals.

In mice with an injection of the rAAV-Cre virus, we detected that they spent significantly less time in the centre than in the corner. Also, they spent significantly less time in the centre than those injected with the rAAV-Venus control virus. This suggests that animals injected with the rAAV-Cre virus are more anxious. Previous studies support these results similarly, showing that the inactivation of genes with roles in memory formation increases anxiety-related behaviour in mice [114]. However, the results in this study are not reliable. First, there is a significant variation between the animals within this group. We optimised the surgery procedure and tested different injection coordinates and viral dilutions to decrease neuronal loss and tissue lesions. This gives individual differences to the animals within the group, making it difficult to analyse this group as a whole. Secondly, many animals from the initial surgery procedures have severe neuronal loss and hippocampal lesions. Consequently, behavioural results for this group do not necessarily say anything about the role of *Tdg* in anxiety, as much as the effect of

hippocampal lesions. Varying degree of infection and hippocampal lesions makes it difficult to say anything about the behaviour of these animals as a collected group. Therefore, after surgery optimisation, I analysed a select group of animals which showed healthy hippocampal tissues around the injection site. In this case, rAAV-Cre-injected animals still spend significantly less time in the centre than in the corner. This result suggests that mice with an injection of the 1:20 rAAV-Cre show an increased level of anxiety. Nevertheless, the selected group consists only of five animals, and more data is needed to conclude any of these findings sufficiently.

Reliability and relevance of results: NOL test

In this study, I found that Naïve LoxP-mini*Tdg* mice spent significantly more time exploring the novel object location above the chance level. This suggests that these animals have normal spatial memory and that the behavioural paradigm works. Studies show that normal mice without memory impairment prefer the novel object location, consistent with our findings.

Results for PBS and rAAV-Venus injected animals show no significant preference for the novel object location. This contradicts our initial hypothesis, in which we expected that the mice injected with PBS and rAAV-Venus control virus behaved similarly to Naïve animals, as none of these animals is affected by Cre-induced *Tdg* depletion. The possible explanations for these results are similar to OFT discussed in section 4.1.3. In short, animals injected with PBS or rAAV-Venus control virus have undergone surgery, as opposed to the Naïve animals. The surgery procedure can have led to infections in the hippocampus or had other impacts on behaviour (e.g. previous handling associated with surgery). The reliability of the results can be questioned, as the variance within the groups is significant. This can be explained by the quality of the surgery procedure (before and after optimisation) for the compared groups.

We found that animals injected with the rAAV-Cre virus spent significantly more time exploring the novel object location than chance level. This is true for the collected group with all rAAV-Cre-virus injected animals and the selected group of animals after surgery optimisation. These results do not support our hypothesis. We expected that animals with hippocampal TDG depletion would display impaired long-term spatial memory. Many animals injected with the rAAV-Cre virus show severe neuronal loss and hippocampal tissue lesions. Previous studies have demonstrated that animals with hippocampal lesions show impaired spatial memory, consistent with the well-accepted notion that the HPC is a part of a memory system important for spatial memory [115]. Thus, we would expect animals injected with the rAAV-Cre virus to show impaired spatial memory, regardless of whether it resulted from TDG depletion of hippocampal lesions.
A possible explanation for why animals do not show impaired spatial memory, despite severe hippocampal lesions, could be their inability to form distinct memory of the novel and familiar object location. When testing long-term memory, animals may consider the non-displayed object (familiar object location) to no longer be familiar, as the mice do not remember the previous experience of the exposure trials. As such, the animal believes that both object locations are novel, as they have not formed a memory of either location during exposure trials. In this way, animals cannot discriminate between the two object locations.

A more likely explanation for the contradictory finding in this study is the low reliability of the results. Results from the collected group with all rAAV-Cre virus injected animals are unreliable, as there are considerable differences between the individual animals within the group. As previously described in section 4.1.3: OFT, these animals are injected with varying viral concentrations and have had an injection at different stages of optimising the surgery procedure. Unexpected, the selected group of animals after surgery optimisation also showed normal spatial memory, showing a preference for the novel object location. However, these results are based on small sample size, and more data must be included to gain statistical power. Also, there are varying degrees of viral infection success in animals injected after surgery optimisation. More animals with a good viral infection must be included in future studies.

Reliability and relevance of results: Y-maze

In this study, I found that Naïve loxP-mini*Tdg* mice and those with PBS and rAAV-Cre injection show a significant preference for exploring the novel arm. Although not significant, rAAV-Venus control virus injected animals prefer the novel arm. As expected, animals without Cre-induced TDG depletion show preferences for the previously unvisited arm. The Naïve animals show a preference for the novel object location above the chance level, indicating that the behavioural paradigm works. Unexpected, mice injected with the rAAV-Cre virus also show preferences for the novel arm. Similarly, as discussed for the OF and NOL test, these results have low reliability due to significant variations within the group, which may cause the results. There is no significant preference for the novel arm above chance for the selected group of animals after surgery optimisation. This random alternation between the familiar and novel arm suggests impairment in spatial memory. This supports our hypothesis. However, larger sample size must be included to confirm these results.

5 Conclusion

In this study, I managed to optimise a virus injection protocol successfully depleting TDG and avoiding neuronal loss and tissue lesions caused by Cre toxicity. Together with colleagues, I established behavioural tasks for long-term memory assessing behaviour of mice with hippocampal TDG depletion. We observed that mice injected with rAAV-Cre are more anxious. It is not clear whether depletion of TDG in hippocampal neurons affects long-term spatial memory, as significant variances within the group were introduced. A selected group of animals with no hippocampal lesion show tendencies of impaired spatial memory in the Y-maze test. However, a larger sample size is needed to conclude any findings. Due to a low consistency in successful TDG depletion by rAAV-Cre injection, we aimed to generate a new brain specific TDG knockout mouse model depleting TDG independent of viral tools. I successfully established a brain specific *Tdg* knockout mouse model (CamKIIα-*Tdg*-KO). This was confirmed by IHC of GFP showing Cre-mediated GFP expression, and presumably *Tdg* depletion, in CA1, CA3 and DG. In future studies, these animals can be used to further explore TDGs role in hippocampal dependent memory.

6 Future perspectives

Additional studies can further explore TDG's role in hippocampal-dependent memory. Several studies would be interesting to follow up on:

1. The optimised protocol can be used to generate more animals with successful TDG depletion and no hippocampal lesions. These animals can subsequently be assessed in behavioural studies to gain statistical power for current findings.

2. We can test other virus variants, such as Split-Cre. This can be done by creating an inactive "split-cre" fragment that regains Cre activity when introducing overlapping co-expression [114]. Cre is split into N-and C-terminal segments (CCre and NCre), and subsequently injected into separate hippocampal hemispheres This enables the targeting of specific hippocampal circuits by introducing the virus into connected regions. Further, Cre toxicity is avoided. I have tested injection of split-Cre in two animals, but the procedure needs to be adequately established and optimised for future studies.

3. We can assess behaviour and cognition using the currently established behaviour protocols (OFT, NOL and Y-maze) using the new mouse model (CamKIIa-*Tdg*-KO). This will give more reliable behavioural results as the hippocampal TDG depletion is more consistent.

4. Different behavioural paradigms such as the radial arm maze or fear conditioning tests can be included to better understand the role of TDG mediated DNA demethylation in memory. The radial arm maze consists of eight arms, and the animal must remember which arms have previously been visited in order to ensure that they do not repeatedly enter arms without a food reward. Visual cues are used to guide the animal toward the location with a reward. In this way, The radial arm maze evaluates spatial learning and working memory [115]. The fear conditioning test assess the ability of mice to learn and remember an association between environmental cues and fear-inducing stimuli. Mice with impairment in memory will not be able to associate a spatial location and fear-inducing stimuli [116]. These tests both use incentives, as opposed to the tests used in this study. The difference in reinforcement may affect the speed of learning and strength of memory [117]. For example, failing to explore an object is not penalised. However, failure to find food reward, or receiving pain, is potentially life-threatening for mice in nature. Thus, these incentives will increase the speed of learning and memory strength [117].

5. In the new mouse model, we can measure the ratio of infected cells to non-infected cells in CA1, CA3 and DG. In this way, we can determine the efficiency of Cre-induced TDG depletion in the different hippocampal subregions for the new mouse model.

6. We could enrich GFP-positive cells from HPC by fluorescence-activated cell sorting (FACS), and assess successful TDG depletion by detecting levels of TDG protein (WB) and mRNA (RT-qPCR).

7. We could measure the level of 5mC, 5hmC, 5fC and 5caC accumulates by Mass Spectrometry (MS) or map the distribution of these oxidative substrates by whole genome sequencing. Previous studies show accumulation of the oxidised derivates 5fC and 5caC after TDG depletion in embryonic stem cells by MS [39]. There were now changes in 5hmC levels, which is not recognised by TDG. This could be interesting to measure for our animals.

7 References

1. Maag, J.L.V., et al., *Widespread promoter methylation of synaptic plasticity genes in long-term potentiation in the adult brain in vivo.* BMC genomics, 2017. **18**(1): p. 250-250.
2. Preston, A.R. and H. Eichenbaum, *Interplay of hippocampus and prefrontal cortex in memory.* Current biology : CB, 2013. **23**(17): p. R764-R773.
3. Gibney, E.R. and C.M. Nolan, *Epigenetics and gene expression.* Heredity, 2010. **105**(1): p. 4-13.
4. Kohli, R.M. and Y. Zhang, *TET enzymes, TDG and the dynamics of DNA demethylation.* Nature, 2013. **502**(7472): p. 472-479.
5. Hamilton, J.P., *Epigenetics: principles and practice.* Digestive diseases (Basel, Switzerland), 2011. **29**(2): p. 130-135.
6. Wu, C.-t. and J.R. Morris, *Genes, Genetics, and Epigenetics: A Correspondence.* Science, 2001. **293**(5532): p. 1103-1105.
7. Portela, A. and M. Esteller, *Epigenetic modifications and human disease.* Nature Biotechnology, 2010. **28**(10): p. 1057-1068.
8. Lister, R., et al., *Human DNA methylomes at base resolution show widespread epigenomic differences.* Nature, 2009. **462**(7271): p. 315-22.
9. Moore, L.D., T. Le, and G. Fan, *DNA Methylation and Its Basic Function.* Neuropsychopharmacology, 2013. **38**(1): p. 23-38.
10. Long, H.K., et al., *Protection of CpG islands from DNA methylation is DNA-encoded and evolutionarily conserved.* Nucleic Acids Res, 2016. **44**(14): p. 6693-706.
11. Antequera, F., *Structure, function and evolution of CpG island promoters.* Cellular and Molecular Life Sciences CMLS, 2003. **60**(8): p. 1647-1658.
12. Boyes, J. and A. Bird, *Repression of genes by DNA methylation depends on CpG density and promoter strength: evidence for involvement of a methyl-CpG binding protein.* Embo j, 1992. **11**(1): p. 327-33.
13. Weber, M. and D. Schübeler, *Genomic patterns of DNA methylation: targets and function of an epigenetic mark.* Current Opinion in Cell Biology, 2007. **19**(3): p. 273-280.
14. Di Croce, L., et al., *Methyltransferase recruitment and DNA hypermethylation of target promoters by an oncogenic transcription factor.* Science, 2002. **295**(5557): p. 1079-82.
15. Brenner, C., et al., *Myc represses transcription through recruitment of DNA methyltransferase corepressor.* Embo j, 2005. **24**(2): p. 336-46.
16. Wang, Y.A., et al., *DNA methyltransferase-3a interacts with p53 and represses p53-mediated gene expression.* Cancer Biol Ther, 2005. **4**(10): p. 1138-43.
17. Nan, X., et al., *Transcriptional repression by the methyl-CpG-binding protein MeCP2 involves a histone deacetylase complex.* Nature, 1998. **393**(6683): p. 386-9.
18. Jørgensen, H.F., I. Ben-Porath, and A.P. Bird, *Mbd1 is recruited to both methylated and nonmethylated CpGs via distinct DNA binding domains.* Mol Cell Biol, 2004. **24**(8): p. 3387-95.

19. Duan, Z. and J. Lu, *DNA Methyltransferases in Depression: An Update.* Frontiers in Psychiatry, 2020. **11**(927).
20. Poon, C.H., L.S.R. Tse, and L.W. Lim, *DNA methylation in the pathology of Alzheimer's disease: from gene to cognition.* Annals of the New York Academy of Sciences, 2020. **1475**(1): p. 15-33.
21. Okano, M., et al., *DNA methyltransferases Dnmt3a and Dnmt3b are essential for de novo methylation and mammalian development.* Cell, 1999. **99**(3): p. 247-57.
22. Bestor, T., et al., *Cloning and sequencing of a cDNA encoding DNA methyltransferase of mouse cells. The carboxyl-terminal domain of the mammalian enzymes is related to bacterial restriction methyltransferases.* J Mol Biol, 1988. **203**(4): p. 971-83.
23. Pradhan, S., et al., *Recombinant Human DNA (Cytosine-5) Methyltransferase: I. EXPRESSION, PURIFICATION, AND COMPARISON OF DE NOVO AND MAINTENANCE METHYLATION*.* Journal of Biological Chemistry, 1999. **274**(46): p. 33002-33010.
24. Ziller, M.J., et al., *Charting a dynamic DNA methylation landscape of the human genome.* Nature, 2013. **500**(7463): p. 477-481.
25. Vanyushin, B.F., et al., *The 5-Methylcytosine in DNA of Rats.* Gerontology, 1973. **19**(3): p. 138-152.
26. Bollati, V., et al., *Decline in genomic DNA methylation through aging in a cohort of elderly subjects.* Mechanisms of Ageing and Development, 2009. **130**(4): p. 234-239.
27. Wu, X. and Y. Zhang, *TET-mediated active DNA demethylation: mechanism, function and beyond.* Nature Reviews Genetics, 2017. **18**(9): p. 517-534.
28. He, S., et al., *Passive DNA demethylation preferentially up-regulates pluripotency-related genes and facilitates the generation of induced pluripotent stem cells.* Journal of Biological Chemistry, 2017. **292**(45): p. 18542-18555.
29. Inoue, A. and Y. Zhang, *Replication-Dependent Loss of 5-Hydroxymethylcytosine in Mouse Preimplantation Embryos.* Science, 2011. **334**(6053): p. 194-194.
30. Hermann, A., H. Gowher, and A. Jeltsch, *Biochemistry and biology of mammalian DNA methyltransferases.* Cellular and Molecular Life Sciences CMLS, 2004. **61**(19): p. 2571-2587.
31. Wu, S.C. and Y. Zhang, *Active DNA demethylation: many roads lead to Rome.* Nature Reviews Molecular Cell Biology, 2010. **11**(9): p. 607-620.
32. Cortellino, S., et al., *Thymine DNA Glycosylase Is Essential for Active DNA Demethylation by Linked Deamination-Base Excision Repair.* Cell, 2011. **146**(1): p. 67-79.
33. Wiebauer, K. and J. Jiricny, *Mismatch-specific thymine DNA glycosylase and DNA polymerase beta mediate the correction of G.T mispairs in nuclear extracts from human cells.* Proceedings of the National Academy of Sciences, 1990. **87**(15): p. 5842-5845.
34. Neddermann, P. and J. Jiricny, *The purification of a mismatch-specific thymine-DNA glycosylase from HeLa cells.* Journal of Biological Chemistry, 1993. **268**(28): p. 21218-21224.
35. Krokan, H.E. and M. Bjørås, *Base excision repair.* Cold Spring Harbor perspectives in biology, 2013. **5**(4): p. a012583-a012583.
36. Tini, M., et al., *Association of CBP/p300 Acetylase and Thymine DNA Glycosylase Links DNA Repair and Transcription.* Molecular Cell, 2002. **9**(2): p. 265-277.
37. Jen, P.H. and C.H. Wu, *Echo duration selectivity of the bat varies with pulse-echo amplitude difference.* Neuroreport, 2008. **19**(3): p. 373-7.

38. Maiti, A. and A.C. Drohat, *Thymine DNA glycosylase can rapidly excise 5-formylcytosine and 5-carboxylcytosine: potential implications for active demethylation of CpG sites.* J Biol Chem, 2011. **286**(41): p. 35334-35338.
39. Schwarz, S.D., et al., *Inducible TDG knockout models to study epigenetic regulation.* F1000Research, 2020. **9**: p. 1112-1112.
40. Onodera, A., et al., *Roles of TET and TDG in DNA demethylation in proliferating and non-proliferating immune cells.* Genome Biology, 2021. **22**(1): p. 186.
41. Aravind, L. and E.V. Koonin, *The alpha/beta fold uracil DNA glycosylases: a common origin with diverse fates.* Genome biology, 2000. **1**(4): p. RESEARCH0007-RESEARCH0007.
42. Coey, C.T., et al., *Structural basis of damage recognition by thymine DNA glycosylase: Key roles for N-terminal residues.* Nucleic Acids Research, 2016. **44**(21): p. 10248-10258.
43. Cortázar, D., et al., *The enigmatic thymine DNA glycosylase.* DNA Repair, 2007. **6**(4): p. 489-504.
44. Sjolund, A.B., A.G. Senejani, and J.B. Sweasy, *MBD4 and TDG: Multifaceted DNA glycosylases with ever expanding biological roles.* Mutation Research/Fundamental and Molecular Mechanisms of Mutagenesis, 2013. **743-744**: p. 12-25.
45. Missero, C., et al., *The DNA Glycosylase T:G Mismatch-specific Thymine DNA Glycosylase Represses Thyroid Transcription Factor-1-activated Transcription.* Journal of Biological Chemistry, 2001. **276**(36): p. 33569-33575.
46. Li, Y.-Q., et al., *Association of Dnmt3a and thymine DNA glycosylase links DNA methylation with base-excision repair.* Nucleic Acids Research, 2006. **35**(2): p. 390-400.
47. Uhlén, M., et al., *Tissue-based map of the human proteome.* Science, 2015. **347**(6220): p. 1260419.
48. Smet-Nocca, C., et al., *The thymine-DNA glycosylase regulatory domain: residual structure and DNA binding.* Biochemistry, 2008. **47**(25): p. 6519-30.
49. Gallinari, P. and J. Jiricny, *A new class of uracil-DNA glycosylases related to human thymine-DNA glycosylase.* Nature, 1996. **383**(6602): p. 735-738.
50. Steinacher, R. and P. Schär, *Functionality of Human Thymine DNA Glycosylase Requires SUMO-Regulated Changes in Protein Conformation.* Current Biology, 2005. **15**(7): p. 616-623.
51. Cortázar, D., et al., *Embryonic lethal phenotype reveals a function of TDG in maintaining epigenetic stability.* Nature, 2011. **470**(7334): p. 419-423.
52. Saito, Y., et al., *Embryonic Lethality in Mice Lacking Mismatch-Specific Thymine DNA Glycosylase Is Partially Prevented by DOPS, a Precursor of Noradrenaline.* The Tohoku Journal of Experimental Medicine, 2012. **226**(1): p. 75-83.
53. Lonergan, M.E., et al., *Time-dependent expression of Arc and zif268 after acquisition of fear conditioning.* Neural Plast, 2010. **2010**: p. 139891.
54. Bekinschtein, P., et al., *Persistence of Long-Term Memory Storage Requires a Late Protein Synthesis- and BDNF- Dependent Phase in the Hippocampus.* Neuron, 2007. **53**(2): p. 261-277.
55. Oliveira, A.M.M., *DNA methylation: a permissive mark in memory formation and maintenance.* Learning & Memory, 2016. **23**(10): p. 587-593.
56. Guo, J.U., et al., *Neuronal activity modifies the DNA methylation landscape in the adult brain.* Nature Neuroscience, 2011. **14**(10): p. 1345-1351.
57. Halder, R., et al., *DNA methylation changes in plasticity genes accompany the formation and maintenance of memory.* Nature Neuroscience, 2016. **19**(1): p. 102-110.

58. Miller, C.A. and J.D. Sweatt, *Covalent Modification of DNA Regulates Memory Formation.* Neuron, 2007. **53**(6): p. 857-869.
59. Levenson, J.M., et al., *Evidence That DNA (Cytosine-5) Methyltransferase Regulates Synaptic Plasticity in the Hippocampus.* Journal of Biological Chemistry, 2006. **281**(23): p. 15763-15773.
60. De Jager, P.L., et al., *Alzheimer's disease: early alterations in brain DNA methylation at ANK1, BIN1, RHBDF2 and other loci.* Nature Neuroscience, 2014. **17**(9): p. 1156-1163.
61. Gavin, D.P. and R.P. Sharma, *Histone modifications, DNA methylation, and Schizophrenia.* Neuroscience & Biobehavioral Reviews, 2010. **34**(6): p. 882-888.
62. LaPlant, Q., et al., *Dnmt3a regulates emotional behavior and spine plasticity in the nucleus accumbens.* Nat Neurosci, 2010. **13**(9): p. 1137-43.
63. Bird, C.M. and N. Burgess, *The hippocampus and memory: insights from spatial processing.* Nature Reviews Neuroscience, 2008. **9**(3): p. 182-194.
64. Man, K., et al., *Neural convergence and divergence in the mammalian cerebral cortex: From experimental neuroanatomy to functional neuroimaging.* Journal of Comparative Neurology, 2013. **521**(18): p. 4097-4111.
65. van Strien, N.M., N.L.M. Cappaert, and M.P. Witter, *The anatomy of memory: an interactive overview of the parahippocampal–hippocampal network.* Nature Reviews Neuroscience, 2009. **10**(4): p. 272-282.
66. Day, J.J. and J.D. Sweatt, *DNA methylation and memory formation.* Nature Neuroscience, 2010. **13**(11): p. 1319-1323.
67. Nakazawa, K., et al., *NMDA receptors, place cells and hippocampal spatial memory.* Nature Reviews Neuroscience, 2004. **5**(5): p. 361-372.
68. Paul, C.-M., G. Magda, and S. Abel, *Spatial memory: Theoretical basis and comparative review on experimental methods in rodents.* Behavioural Brain Research, 2009. **203**(2): p. 151-164.
69. Lagali, P., C. Corcoran, and D. Picketts, *Hippocampus development and function: role of epigenetic factors and implications for cognitive disease.* Clinical Genetics, 2010. **78**(4): p. 321-333.
70. Squire, L.R., C.E. Stark, and R.E. Clark, *The medial temporal lobe.* Annu Rev Neurosci, 2004. **27**: p. 279-306.
71. Lee, J.K., E.G. Johnson, and S. Ghetti, *Hippocampal Development: Structure, Function and Implications*, in *The Hippocampus from Cells to Systems: Structure, Connectivity, and Functional Contributions to Memory and Flexible Cognition*, D.E. Hannula and M.C. Duff, Editors. 2017, Springer International Publishing: Cham. p. 141-166.
72. van Strien, N.M., N.L. Cappaert, and M.P. Witter, *The anatomy of memory: an interactive overview of the parahippocampal-hippocampal network.* Nat Rev Neurosci, 2009. **10**(4): p. 272-82.
73. Stepan, J., J. Dine, and M. Eder, *Functional optical probing of the hippocampal trisynaptic circuit in vitro: network dynamics, filter properties, and polysynaptic induction of CA1 LTP.* Front Neurosci, 2015. **9**: p. 160.
74. Steward, O., *Topographic organization of the projections from the entorhinal area to the hippocampal formation of the rat.* J Comp Neurol, 1976. **167**(3): p. 285-314.
75. Chronister, R.B. and J.F. DeFrance, *Organization of projection neurons of the hippocampus.* Experimental Neurology, 1979. **66**(3): p. 509-523.
76. Nicoll, R.A. and D. Schmitz, *Synaptic plasticity at hippocampal mossy fibre synapses.* Nature Reviews Neuroscience, 2005. **6**(11): p. 863-876.

77. Köhler, C., *Intrinsic connections of the retrohippocampal region in the rat brain. II. The medial entorhinal area.* J Comp Neurol, 1986. **246**(2): p. 149-69.
78. Cenquizca, L.A. and L.W. Swanson, *Spatial organization of direct hippocampal field CA1 axonal projections to the rest of the cerebral cortex.* Brain research reviews, 2007. **56**(1): p. 1-26.
79. Moser, E.I., *The multi-laned hippocampus.* Nature Neuroscience, 2011. **14**(4): p. 407-408.
80. Sharma, S., S. Rakoczy, and H. Brown-Borg, *Assessment of spatial memory in mice.* Life sciences, 2010. **87**(17-18): p. 521-536.
81. Vorhees, C.V. and M.T. Williams, *Assessing spatial learning and memory in rodents.* ILAR journal, 2014. **55**(2): p. 310-332.
82. Garcia-Alvarez, G., et al., *Impaired spatial memory and enhanced long-term potentiation in mice with forebrain-specific ablation of the Stim genes.* Frontiers in Behavioral Neuroscience, 2015. **9**.
83. Grant, S.G., et al., *Impaired long-term potentiation, spatial learning, and hippocampal development in fyn mutant mice.* Science, 1992. **258**(5090): p. 1903-10.
84. Silva, A.J., et al., *Impaired spatial learning in alpha-calcium-calmodulin kinase II mutant mice.* Science, 1992. **257**(5067): p. 206-11.
85. Sengupta, R., et al., *Viral Cre-LoxP tools aid genome engineering in mammalian cells.* Journal of Biological Engineering, 2017. **11**(1): p. 45.
86. Sauer, B. and N. Henderson, *Site-specific DNA recombination in mammalian cells by the Cre recombinase of bacteriophage P1.* Proceedings of the National Academy of Sciences, 1988. **85**(14): p. 5166-5170.
87. Orban, P.C., D. Chui, and J.D. Marth, *Tissue- and site-specific DNA recombination in transgenic mice.* Proceedings of the National Academy of Sciences, 1992. **89**(15): p. 6861-6865.
88. Tsien, J.Z., et al., *Subregion- and Cell Type–Restricted Gene Knockout in Mouse Brain.* Cell, 1996. **87**(7): p. 1317-1326.
89. Saunders, A., C. Johnson, and B. Sabatini, *Novel recombinant adeno-associated viruses for Cre activated and inactivated transgene expression in neurons.* Frontiers in Neural Circuits, 2012. **6**.
90. Kügler, S., E. Kilic, and M. Bähr, *Human synapsin 1 gene promoter confers highly neuron-specific long-term transgene expression from an adenoviral vector in the adult rat brain depending on the transduced area.* Gene Therapy, 2003. **10**(4): p. 337-347.
91. Botterill, J.J., et al., *Off-Target Expression of Cre-Dependent Adeno-Associated Viruses in Wild-Type C57BL/6J Mice.* eneuro, 2021. **8**(6): p. ENEURO.0363-21.2021.
92. Mayford, M., et al., *The 3′-untranslated region of CaMKIIα is a cis-acting signal for the localization and translation of mRNA in dendrites.* Proceedings of the National Academy of Sciences, 1996. **93**(23): p. 13250-13255.
93. Burgin, K., et al., *In situ hybridization histochemistry of Ca2+/calmodulin-dependent protein kinase in developing rat brain.* The Journal of Neuroscience, 1990. **10**(6): p. 1788-1798.
94. Au - Denninger, J.K., B.M. Au - Smith, and E.D. Au - Kirby, *Novel Object Recognition and Object Location Behavioral Testing in Mice on a Budget.* JoVE, 2018(141): p. e58593.

95. Sanderson, D.J., et al., *Enhanced long-term and impaired short-term spatial memory in GluA1 AMPA receptor subunit knockout mice: evidence for a dual-process memory model.* Learn Mem, 2009. **16**(6): p. 379-86.
96. Kang, W., et al., *Astrocyte activation is suppressed in both normal and injured brain by FGF signaling.* Proceedings of the National Academy of Sciences, 2014. **111**(29): p. E2987-E2995.
97. Cheng, X., et al., *Morphological and functional alterations of astrocytes responding to traumatic brain injury.* JIN, 2019. **18**(2): p. 203-215.
98. Gusel'nikova, V.V. and D.E. Korzhevskiy, *NeuN As a Neuronal Nuclear Antigen and Neuron Differentiation Marker.* Acta naturae, 2015. **7**(2): p. 42-47.
99. Choleris, E., et al., *A detailed ethological analysis of the mouse open field test: effects of diazepam, chlordiazepoxide and an extremely low frequency pulsed magnetic field.* Neuroscience & Biobehavioral Reviews, 2001. **25**(3): p. 235-260.
100. Dinel, A.-L., et al., *Cognitive and Emotional Alterations Are Related to Hippocampal Inflammation in a Mouse Model of Metabolic Syndrome.* PLoS ONE, 2011. **6**(9): p. e24325.
101. *Cre-recombinase-associated toxicity highlights limitations of genome editing.* Disease Models & Mechanisms, 2013. **6**(6): p. 1299-1300.
102. Forni, P.E., et al., *High levels of Cre expression in neuronal progenitors cause defects in brain development leading to microencephaly and hydrocephaly.* The Journal of neuroscience : the official journal of the Society for Neuroscience, 2006. **26**(37): p. 9593-9602.
103. Rezai Amin, S., et al., *Viral vector-mediated Cre recombinase expression in substantia nigra induces lesions of the nigrostriatal pathway associated with perturbations of dopamine-related behaviors and hallmarks of programmed cell death.* Journal of Neurochemistry, 2019. **150**(3): p. 330-340.
104. Loonstra, A., et al., *Growth inhibition and DNA damage induced by Cre recombinase in mammalian cells.* Proceedings of the National Academy of Sciences, 2001. **98**(16): p. 9209-9214.
105. Thyagarajan, B., et al., *Mammalian genomes contain active recombinase recognition sites.* Gene, 2000. **244**(1): p. 47-54.
106. Sharma, S. and J. Zhu, *Immunologic applications of conditional gene modification technology in the mouse.* Current protocols in immunology, 2014. **105**: p. 10.34.1-10.34.13.
107. Heffner, C.S., et al., *Supporting conditional mouse mutagenesis with a comprehensive cre characterization resource.* Nature Communications, 2012. **3**(1): p. 1218.
108. Choi, C.-I., et al., *Simultaneous deletion of floxed genes mediated by CaMKIIα-Cre in the brain and in male germ cells: application to conditional and conventional disruption of Goα.* Experimental & molecular medicine, 2014. **46**(5): p. e93-e93.
109. Deacon, R.M.J. and J.N.P. Rawlins, *T-maze alternation in the rodent.* Nature Protocols, 2006. **1**(1): p. 7-12.
110. Kraeuter, A.K., P.C. Guest, and Z. Sarnyai, *The Y-Maze for Assessment of Spatial Working and Reference Memory in Mice.* Methods Mol Biol, 2019. **1916**: p. 105-111.
111. Seibenhener, M.L. and M.C. Wooten, *Use of the Open Field Maze to measure locomotor and anxiety-like behavior in mice.* Journal of visualized experiments : JoVE, 2015(96): p. e52434-e52434.

112. Vogel-Ciernia, A. and M.A. Wood, *Examining Object Location and Object Recognition Memory in Mice.* Current Protocols in Neuroscience, 2014. **69**(1): p. 8.31.1-8.31.17.
113. Sestakova, N., et al., *Determination of motor activity and anxiety-related behaviour in rodents: methodological aspects and role of nitric oxide.* Interdisciplinary toxicology, 2013. **6**(3): p. 126-135.
114. Bats, S., et al., *The effects of a mild stressor on spontaneous alternation in mice.* Behavioural Brain Research, 2001. **118**(1): p. 11-15.
115. Eltokhi, A., B. Kurpiers, and C. Pitzer, *Behavioral tests assessing neuropsychiatric phenotypes in adolescent mice reveal strain- and sex-specific effects.* Scientific Reports, 2020. **10**(1): p. 11263.
116. Brown, R.E., L. Stanford, and H.M. Schellinck, *Developing Standardized Behavioral Tests for Knockout and Mutant Mice.* ILAR Journal, 2000. **41**(3): p. 163-174.

8 Appendix

Table 1. Primer sequences for PCR reactions

Allele	Primer	Sequence	Product size
Tdg WT	GT TDG D Forward	TTGCGTGGGAGTAACCGAGC	0.6 kb
	GT TDG B Reverse	GATGCACTCGGGAGACTTACAG	
*mini*Tdg	Compl Forward	AAATACTCTGAGTCCAAACCGGG	0.65 kb
	TDG C Reverse	TGGTGAATCCGATGCCGTACTTG	
CAG-gfp	CAG-St-eGFP-Forward	CTTCAGCCGCTACCCCGACCACA	0.5 kb
	CAG-St-eGFP-Reverse	ATCGCGCTTCTCGTTGGGGTCTTT	
CamKIIα-Cre	JAX_10884_Forward	GTTCTCCGTTTGCACTCAGG	0.3 kb
	JAX_oIMR8990_Reverse	CAGGTTCTTGCGAACCTCAT	

Table 2. Primary antibodies

Primary Antibody	Isotype	Dilution	Host	Manufacturer	Catalog number	Function/Cell type marker
NeuN	mIgG1	1:500		Millipore	MAB377	Neuron nucleic marker.
GFP	mIgG2 rIgG	1:1000 1:1000		Thermo Fisher Invitrogen	A-11120 A-11122	Gene reporter. Show Cre-induced GFP expression.
GFAP	mIgG1	1:5000		Cell signalling	3670S	Astrocytes Marker for immune response.

Table 3. Secondary antibodies

Secondary Antibody	Isotype	Host	Dilution	Manufacturer	Catalog number	Function/Cell type marker
A647	mIgGl		1:1000	Invitrogen	A-21241	
A488	mIgG2a mIgG1 rIgG		1:1000	Invitrogen	A-21131 A-21121 A-11008	
A555	rIgG		1:1000	Invitrogen	A-21241	

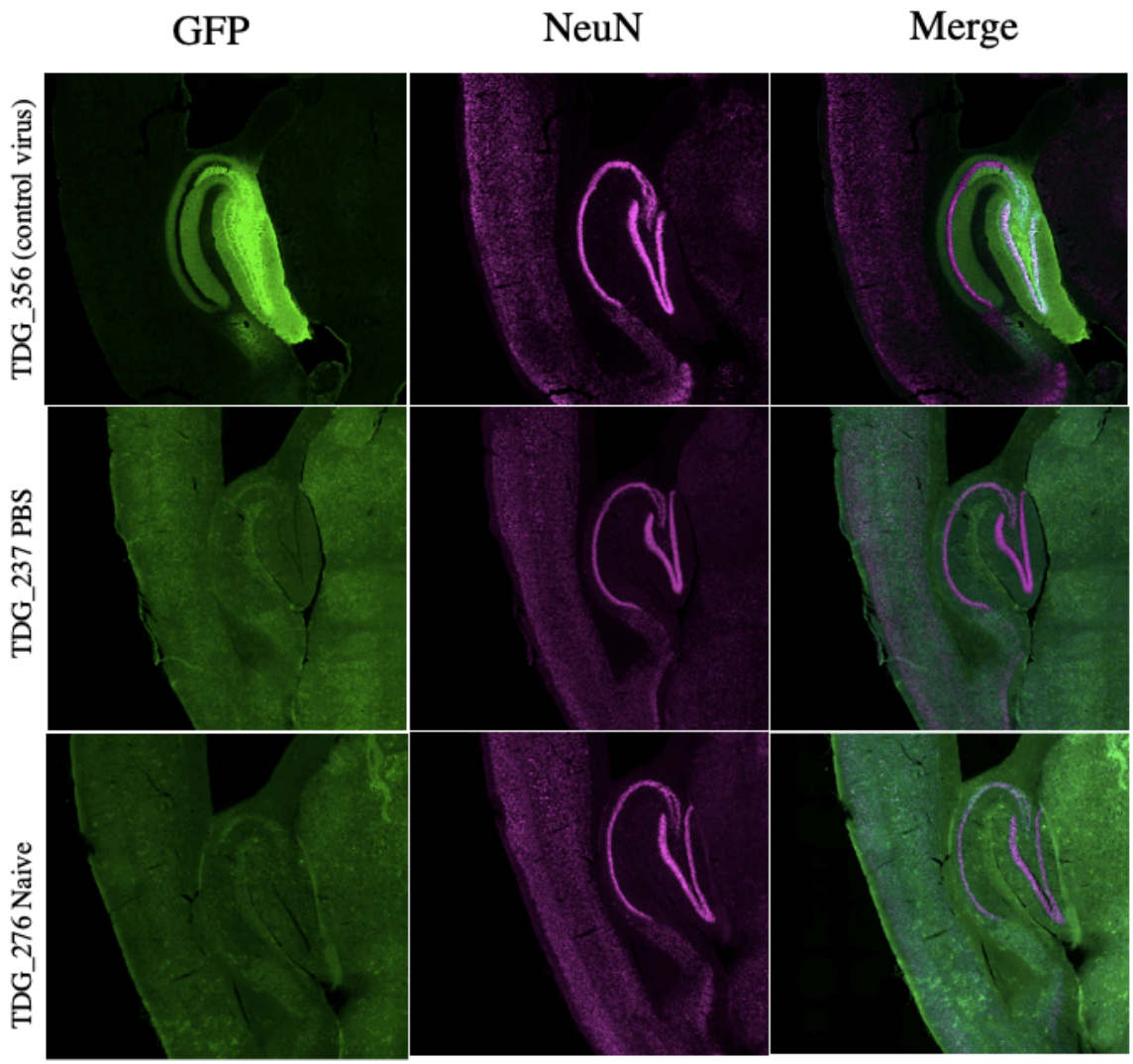

Figure 15. Cre induced GFP expression, neuronal loss by NeuN expression following rAAV-Cre injection.

The image show GFP (green) and NeuN (Magenta) stained hippocampal regions (30µm, Axioscan from Zeiss). Three representative images of loxP-miniTdg mice show lack of GFP expression, neuronal loss and tissue lesions following the injection of PBS and rAAV-Venus or for non-injected (Naïve). e.g., TDG_276 is a non-injected Naïve animal, displaying no GFP expression or neuronal loss. TDG_337 is injected with PBS, and show no GFP expression or neuronal loss. TDG_356 is injected with rAAV-Venus, and show no GFP expression or Neuronal loss. Venus is a YFP protein and could be visualized using the anti-GFP antibody. Staining performed by Konsanse Skogøy Innvær. Images processed in Zen software (Zeiss).

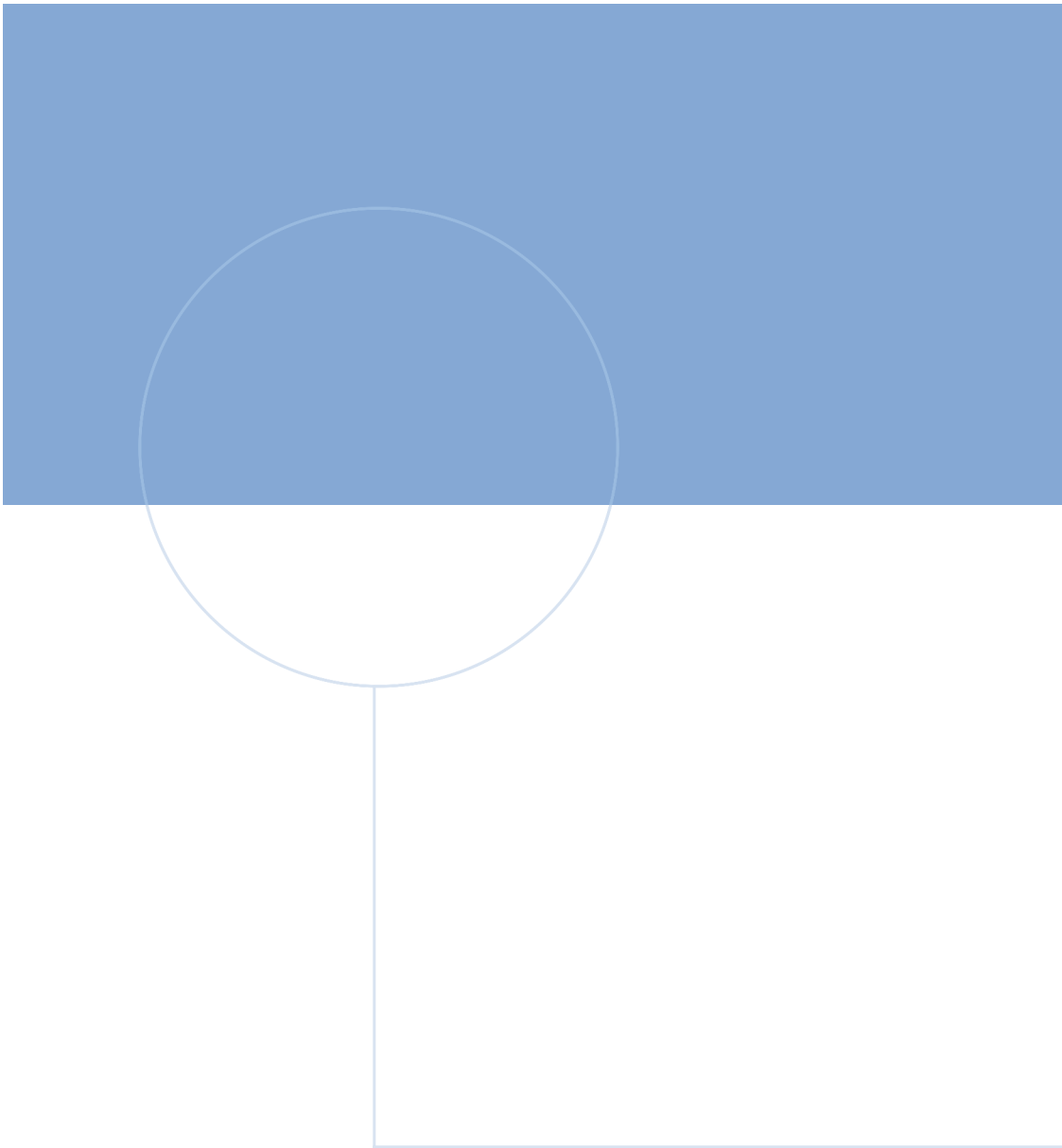

NTNU

Norwegian University of
Science and Technology